



## City Research Online

### City, University of London Institutional Repository

---

**Citation:** Ballotta, L. & Grégory, R. (2022). Smiles & Smirks: Volatility and leverage by jumps. *European Journal of Operational Research*, 298(3), pp. 1145-1161. doi: 10.1016/j.ejor.2021.08.023

This is the accepted version of the paper.

This version of the publication may differ from the final published version.

---

**Permanent repository link:** <https://openaccess.city.ac.uk/id/eprint/26594/>

**Link to published version:** <https://doi.org/10.1016/j.ejor.2021.08.023>

**Copyright:** City Research Online aims to make research outputs of City, University of London available to a wider audience. Copyright and Moral Rights remain with the author(s) and/or copyright holders. URLs from City Research Online may be freely distributed and linked to.

**Reuse:** Copies of full items can be used for personal research or study, educational, or not-for-profit purposes without prior permission or charge. Provided that the authors, title and full bibliographic details are credited, a hyperlink and/or URL is given for the original metadata page and the content is not changed in any way.

---

---

---

City Research Online:

<http://openaccess.city.ac.uk/>

[publications@city.ac.uk](mailto:publications@city.ac.uk)

---

# Smiles & Smirks: Volatility and leverage by jumps

Laura Ballotta<sup>(a)\*</sup> and Grégory Rayée<sup>(b)</sup>

<sup>(a)</sup>Faculty of Finance, Bayes Business School (formerly Cass), City, University of London  
106 Bunhill Row, London, EC1Y 8TZ, United Kingdom; Email: L.Ballotta@city.ac.uk

<sup>(b)</sup>ALM Analytics, Belfius Banque & Assurances

11 Place Rogier, RT 17-03, 1210 Brussels, Belgium; Email: gregory.rayee@belfius.be

August 2021

## Abstract

We propose a novel flexible framework for the joint evolution of stock log-returns and their volatility based on time changed Lévy process. The novelty of the approach stems from the generality of the jump structure we endow our model with, and the ability of the model to generate leverage effects out of the pure jump component. We derive the characteristic function and the forward characteristic function of the log-returns, which allow for the efficient pricing of vanilla and forward-start-like option contracts by Fourier transform methods. The proposed framework achieves robust calibration performance properties especially in the case of pure jump specifications. The results offered in this paper could have potentially interesting implications in terms of design of models and hedging strategies, and their development.

**Keywords:** Finance; Lévy process; time change; option pricing; dependence.

**JEL Classification:** C51, D52, D53, G12, G13

## 1 Introduction

An extensive empirical literature has documented that stylized features of equity log-returns include, amongst others, the non-normality of their distribution due to evidence of skewness and excess kurtosis, the stochastic evolution over time of their volatility, and the so-called leverage effect, i.e. the (negative) correlation between log-returns and their variance. Numerous attempts to develop generalizations of the Black and Scholes (1973) paradigm have appeared in the literature, by allowing the inclusion of either randomness in the log-returns volatility or jumps or both. Stochastic volatility models began to appear relatively soon after the Black and Scholes (1973) model, amongst which we mention the Heston (1993) model due to its high level of parsimony, tractability and robust out-of-sample performance. Jumps-based models were introduced as well soon after Black and Scholes (1973), starting from Merton (1976) to more recent contributions such as Carr and Wu (2004) amongst others.

From the point of view of the financial industry, the usefulness of sophisticated option pricing models is measured primarily by the accuracy with which they can represent the market implied

---

\*Corresponding Author: L.Ballotta@city.ac.uk

A revised version of this article is forthcoming in the European Journal of Operational Research published by Elsevier.

volatility surface and its dynamics over time. Indeed, as in real life delta-hedging is not sufficient due to higher order risk terms, such as the gamma effect, the book of options - both vanilla and exotics - is usually hedged with other (vanilla) options (see for example Bergomi, 2015, for more details), and hence the attention to the calibration error of the model with respect to the quotes of traded options. Additional identifiers of suitable models include, amongst others, the ability to generate flexible forward smile patterns which allow to satisfactorily price exotic contracts such as forward start options (and the closely related cliquet structures). For example, Schoutens et al. (2005) document a relatively flat forward smile originating out of the Heston (1993) model, which might lead to significantly underprice these contracts.

The main purpose of this paper is to develop a family of joint models for the processes of the stock log-returns and their volatility consistent with vanilla options market quotes, and based on time changed Lévy processes (TCLPs) in the spirit of Carr et al. (2003), Carr and Wu (2004), Huang and Wu (2004), Carr and Wu (2017). In contrast to these contributions, though, our proposed construction is fairly general as it enables the generation of (stochastic) volatility and (stochastic) leverage through jumps as well as diffusion processes, and can be augmented for multiple stochastic volatility factors in a straightforward manner. Indeed, the novelty of our approach stems from the ability to generate dependence effects from pure jump processes, by means of both time varying jump intensity and distributions. The model retains a high level of mathematical tractability as the relevant characteristic functions, which enable option pricing, calibration and risk management are accessible for a relatively large number of specifications.

Further, the proposed setup allows for rich dynamics by both discontinuous movements, i.e. jumps, and stochastic volatility features which can accommodate the levels of skewness and excess kurtosis observed in financial data over both short and long horizons (see Aït-Sahalia, 2004, for example). This additional distribution flexibility can prove very important in reducing any potential mispricing of forward volatility dependent products as well, which is exemplified in general by more convex forward volatility surfaces. Finally, the model remains interpretable as it is possible to identify which parameter accounts for which change in the asset price dynamics.

In light of the practical interest in calibration errors discussed above, in this paper we focus on the calibration to vanilla options quotes and the resulting performance of a general family of models in terms of reproducing implied volatility surfaces over time. We refer to the equity market in which options represent the most actively traded product: in 2018 single stock options and stock index options accounted respectively for 32.6% and 31.6% of the total equity derivatives volume, and OTC contracts accounted for up to 55% of the notional amount outstanding (WFE, 2019, BIS, 2019).

The proposed setup encompasses a large number of models available in the literature, such as Heston (1993), Bates (1996), Barndorff-Nielsen and Shephard (2003), Pan (2002), Eraker et al. (2003), Eraker (2004), Sepp (2008) just to mention a few. It is important though to distinguish our work from that of these contributions: although the large majority of the stochastic volatility models in the literature restricts the behaviour of jumps to compound Poisson processes (see Duffie et al., 2000, as well) and includes them mainly in the dynamics of the log-returns, our model uses a very general structure for the jumps, and incorporates them also in the dynamics of the relevant volatility process.

We achieve this by means of discontinuous processes built out of the family of tempered stable

distributions (for an overview, we refer to Fallahgoul and Loeper, 2019, and references therein), exploiting the very rich ‘fine structure’ (in the sense of Carr et al., 2002) offered by these processes, with jumps spanning from finite activity to infinite variation. This feature allows us to ‘learn’ from market quotes the nature of the infinitely small changes in the log-returns which fill the gaps between the very infrequent big jumps, potentially suggesting the need to substitute the Brownian motion component.

Thus, our paper promotes the general meaning of ‘jump’ as discontinuous movements associated with small and intermediate sizes occurring with high frequency, and not just rare ‘crashes’ (which usually the word ‘jump’ evokes in the collective mind). In other words, our focus is on more agile distributions for the log-returns, which are able to capture the actual levels of skewness and excess kurtosis, and their evolution over time in a flexible and parsimonious manner, moving beyond the long standing ‘dichotomy’ between stochastic volatility and jumps. Indeed the evidence put forward by Eberlein and Keller (1995), Huang and Wu (2004), and Ornathanalai (2014), to mention a few, highlights the superior performance of jumps of small size occurring with high frequency, which could be mis-identified as diffusions, as opposed to rare changes with much larger severities, i.e. low frequency compound Poisson jump specifications.

We summarize the main contributions of this paper as follows.

First, we show how leverage can be introduced in a stochastic volatility model exclusively by means of purely discontinuous processes. This allows us to identify, out of the given general setting, an efficient and parsimonious model devoid of diffusion components, and characterised by infinite variation, i.e. jumps of small size occurring with high frequency, and self-exciting structure, as any change in the driving process simultaneously affects the log-return process, its variance and the intensity of future adverse changes. This model could be considered as the pure jump version of the Heston (1993) model - hence we christened it ‘JH’ model.

Second, we provide useful results for both the characteristic and forward characteristic functions of all models encompassed by our general setting, which are necessary for the pricing of derivative contracts, such as options and skew dependent products.

Third, we test the robustness of our results in a number of directions. To begin with, we find that the JH specification offers robust performance in portraying the joint dynamics of the underlying security and its associated volatility surface. Further, we show the ability of the JH model in reproducing the dynamics of the volatility surface over time by updating a minimal number of parameters, and in originating plausible patterns for the forward volatility smile.

Fourth, we highlight the potential implications of our results at managerial level. Indeed, our analysis can provide indications regarding which model feature(s) needs to be prioritized, as it shows the importance of both discontinuous risk factors as drivers for both log-returns and their variance, and features such as stochastic volatility of volatility, covariance and leverage in enabling the model to fit the data better. This last point is of particular significance in view of possible extensions of the model to the multivariate case in order to maintain a parsimonious dimensional complexity of the parameter space.

Finally, we note that the ability of the proposed construction to generate more realistic forward smile patterns could be relevant towards model risk reduction; in this sense the analysis offered in this paper shows that risk management considerations need to include not just the risk of a (rare) crash, but also and most importantly risk of (very frequent) small and intermediate sized

jumps.

The paper is organised as follows. The preliminary concepts on TCLPs and the general framework for the financial model are offered in Sections 2 and 3 respectively. The empirical performance of different model specifications catered by the proposed setup is illustrated in Section 4. Section 5 offers some concluding remarks. Detailed mathematical proofs are deferred to Appendix A in the online supplementary material.

## 2 Background: time changed Lévy processes

### 2.1 From Lévy processes to time changed Lévy processes

A Lévy process,  $L(t)$ , on a filtered probability space  $(\Omega, \mathbb{F}, \{\mathbb{F}_t\}_{t \geq 0}, \mathbb{P})$  is a continuous time process with independent and stationary increments, whose distribution is infinitely divisible, so that its characteristic function is  $\phi(u; t) = e^{t\varphi(u)}$ ,  $u \in \mathbb{R}$  with

$$\varphi(u) = i\alpha u - \frac{u^2}{2}\sigma^2 + \int_{\mathbb{R}} (e^{iux} - 1 - iux1_{|x| \leq 1}) \nu(dx),$$

where  $\alpha \in \mathbb{R}$ ,  $\sigma \in \mathbb{R}^+$  and  $\nu$  is a positive measure on  $\mathbb{R}$  such that

$$\nu(\{0\}) = 0, \quad \int_{\mathbb{R}} (|x|^2 \wedge 1) \nu(dx) < \infty.$$

The triplet  $(\alpha, \sigma^2, \nu(dx))$  represents the generating triplet, or differential characteristics denoted as  $\partial\Pi(L|\mathbb{P})$ , of  $L(t)$  and  $\varphi(\cdot)$  denotes the characteristic exponent.

As the core of the application is option pricing, the following assumption is required to ensure that any risk neutral martingale measure is well defined (see for example Eberlein, 2013 and references therein).

**Assumption 1** *There exists a constant  $M > 1$  such that*

$$\int_{|x|>1} e^{ux} \nu(dx) < \infty \quad \text{for all } u \in [-M, M], \quad (1)$$

*i.e. the exponential moment of the first order of  $L$  is finite.*

Time changed Lévy processes (TCLP) are obtained by observing the Lévy process  $L(t)$ , the so called base process, on a time scale governed by a stochastic clock, i.e. a non-negative, non-decreasing stochastic process  $T(t)$ , which is right-continuous with left limits satisfying the usual regularity conditions. Specifically, we assume that  $T(t)$  is an absolutely continuous finite time change, i.e. a process defined by the pathwise integral

$$T(t) = \int_0^t v(s) ds, \quad (2)$$

where  $v(t)$  is a positive càdlàg process representing the instantaneous activity rate of the clock. Further, we assume the following holds (see Küchler and Sørensen, 1997, for example)

**Assumption 2** *The time change  $T(t)$  is  $L$ -continuous, i.e.  $L$  is constant on all intervals  $[T(u-), T(u)]$ ,  $u > 0$ .*

Then  $X(t) = L(T(t))$  is a TCLP with differential characteristics  $\partial\Pi(L|\mathbb{P}) = (\alpha v(t_-), \sigma^2 v(t_-), \nu(dx)v(t_-))$  (see Eberlein and Kallsen, 2019, and references therein). This construction recognizes that price changes are caused by imbalances in demand and supply due to trades. Thus uncertainty originates from the timing of the change and its magnitude. The former is modelled by the clock  $T(t)$ , which can be interpreted as business time, the latter is captured by the base process  $L(t)$ .

In what follows we assume that the process of the integrated variance is given by the predictable quadratic variation process, which for the given TCLP  $X(t)$  is

$$\langle X \rangle(t) = \text{Var}(L(1)) \int_0^t v(s) ds$$

(see Carr et al., 2003, for example). Further, we define the (squared) volatility process as

$$V(t) = \text{Var}(L(1))v(t), \tag{3}$$

so that  $\int_0^t V(s) ds = \langle X \rangle(t)$ . Assumption 1 guarantees that all of the above are well defined (see Kallsen et al., 2011, as well). Thus, the activity rate  $v(t)$  controls the variance process of  $X(t)$  as the clock  $T(t)$  represents its integrated variance: the faster the clock ticks (i.e. the more active the market is), the higher the volatility. In this respect, the time change of Lévy processes is a tool to equip this class of processes with stochastic volatility features (see also Carr et al., 2003).

Following the same line of reasoning, as long as  $v(t)$  has finite moments, we can define the process  $q(t)$  such that

$$\int_0^t q(s) ds = \langle V \rangle(t) = \text{Var}^2(L(1))\langle v \rangle(t), \tag{4}$$

and the ‘instantaneous covariance’ process  $C(t)$  such that

$$\int_0^t C(s) ds = \langle X, V \rangle(t) = \text{Var}(L(1))\langle X, v \rangle(t). \tag{5}$$

Therefore, the activity rate  $v(t)$  also controls the processes  $q(t)$  and  $C(t)$ , which in the context of option pricing represent the (squared) volatility of volatility and the so-called leverage effect, i.e. the observed tendency of an asset’s volatility to be (negatively) correlated with the asset’s returns. In particular, we note that  $X(t)$  presents stochastic volatility of volatility if the increments of the activity rate have stochastic conditional variance, and leverage is present if the base process and the time change are dependent on each other. More detailed expressions for  $V(t)$ ,  $q(t)$  and  $C(t)$  depend on the specific assumptions concerning the process  $v(t)$  and how dependence is captured.

## 2.2 Characteristic function and the leverage-neutral measure

For financial applications, we require the knowledge of the characteristic function of the process  $X(t)$ ,  $\phi_X(u; t) = \mathbb{E}(e^{iuL(T(t))})$ ,  $u \in \mathbb{R}$ . Under the assumption of a stochastic clock independent of the base process, the characteristic function reduces to  $\phi_X(u; t) = \phi_T(-i\varphi(u); t)$ . For the general case in which the base process and time change are dependent one of the other, the characteristic function can be recovered by a change of measure to the so-called leverage-neutral measure  $\mathbb{M}$  developed by Carr and Wu (2004). This measure  $\mathbb{M}$ , which is absolutely continuous with respect

to  $\mathbb{P}$ , is defined by the complex-valued exponential martingale

$$M_u(t) = e^{iuX(t) - \varphi(u)T(t)}$$

and aims at removing, so to speak, dependence from the model. Then

$$\begin{aligned} \phi_X(u; t) &= \mathbb{E} \left( M_u(t) e^{\varphi(u)T(t)} \right) \\ &= \mathbb{E}^{\mathbb{M}} \left( e^{\varphi(u)T(t)} \right) = \phi_T^{\mathbb{M}}(-i\varphi(u); t) \end{aligned}$$

(for full details we refer to Carr and Wu, 2004, Huang and Wu, 2004).

Thus, regardless of the dependence in place, the characteristic function of the TCLP  $X(t)$  reduces to the characteristic function of the time change  $T(t)$ , which is tractable under specific assumptions for the dynamics of the process chosen as activity rate,  $v(t)$ . A possible choice is the family of affine processes (see Duffie et al., 2000, Kallsen, 2006, for example), which is the case considered in this note; alternative specifications could include linear quadratic models as in Cheng and Scaillet (2007), Santa-Clara and Yan (2010), and Li and Wu (2019), for example.

Finally, we observe that under Assumption 2 the dynamics under the  $\mathbb{M}$ -measure of the process  $X(t)$  can be recovered from the one of the base Lévy process  $L(t)$  (see Küchler and Sørensen, 1997). As the  $\mathbb{M}$ -measure is of Esscher type, standard results (see also Eberlein and Kallsen, 2019, for example) imply that the characteristic exponent of  $L(t)$  under  $\mathbb{M}$  satisfies

$$\varphi^{\mathbb{M}, u}(z) = \varphi(z + u) - \varphi(u), \quad u, z \in \mathbb{R} \quad (6)$$

(for ease of notation, we drop the superscript  $u$  when the meaning is clear). The corresponding dynamics follow directly. Unless otherwise stated, all the assumptions listed in this section hold throughout the rest of the paper.

### 3 Log-returns, stochastic volatility and leverage effects

In this section we provide a general setup for the financial market, we analyse its features and we discuss possible subclasses of models. After deriving the required characteristic functions, we present the extension to a multifactor stochastic volatility setting.

#### 3.1 The market model

Consider a stock price process of the form  $S(t) = S(0)e^{(r-q)t + X(t)}$  under a risk neutral pricing measure<sup>1</sup>  $\mathbb{P}$ , for  $r \geq \bar{r}$  the continuously compounded interest rate (with suitably chosen lower bound  $\bar{r}$ ),  $q \geq 0$  the dividend yield, and  $X(t)$  a semimartingale process, with  $X(0) = 0$ . Further, let  $T(t)$  be a stochastic clock governed by the activity rate  $v(t)$  - see equation (2).

Although other choices are possible, in the following we assume a joint affine specification for  $(v(t), X(t))$ , which allows for known characteristic function of the clock  $T(t)$ , maintaining the tractability of the model. Consequently, we also assume that all the admissibility conditions in

---

<sup>1</sup>We note that the proposed market model is incomplete and consequently the risk neutral martingale measure is not unique. Hence, we follow standard practice for incomplete markets and fix the risk neutral measure through the prices of derivative contracts traded in the market.

Kallsen (2006) are satisfied. Thus, for  $v(0) > 0$  denoting the initial value of the activity rate,

$$v(t) = v(0) + Y_0(t) + Y_1(T(t)) \quad (7)$$

$$X(t) = L_0(t) + L_1(T(t)), \quad (8)$$

for Lévy process  $Y_j(t), L_j(t), j = 0, 1$ , satisfying the stochastic differential equations

$$dY_0(t) = \kappa\theta dt - \eta_{0,J}d\tilde{J}_0(t), \quad \eta_{0,J} \geq 0 \quad (9)$$

$$dY_1(t) = -\kappa dt + \eta_{1,D}dZ_1(t) - \eta_{1,J}d\tilde{J}_1(t), \quad \eta_{1,D}, \eta_{1,J} \geq 0 \quad (10)$$

$$dL_0(t) = -\varphi_0(-i)dt + \sigma_{0,J}dJ_0(t), \quad \sigma_{0,J} \in \mathbb{R}, \quad (11)$$

$$dL_1(t) = -\varphi_1(-i)dt + \sigma_{1,D}dW_1(t) + \sigma_{1,J}dJ_1(t), \quad \sigma_{1,D} \geq 0, \sigma_{1,J} \in \mathbb{R}, \quad (12)$$

with

$$\begin{aligned} \varphi_0(u) &= \varphi_{J_0}(\sigma_{0,J}u), \quad u \in \mathbb{R} \\ \varphi_1(u) &= -\frac{u^2}{2}\sigma_{1,D}^2 + \varphi_{J_1}(\sigma_{1,J}u), \quad u \in \mathbb{R}. \end{aligned}$$

It follows that the characteristic exponent of  $L_j(t)$  is

$$\varphi_{L_j}(u) = -iu\varphi_j(-i) + \varphi_j(u) \quad j = 0, 1, \quad u \in \mathbb{R}. \quad (13)$$

### 3.1.1 A detailed look at the model features

In equations (7)–(12),  $W_1(t)$  is a standard Brownian motion, and  $J_j(t), j = 0, 1$  are independent pure jump Lévy processes with characteristic exponent  $\varphi_{J_j}(u)$  and triplets  $\partial\Pi(J_j|\mathbb{P}) = (\alpha_j, 0, \nu_j(dx))$ ,  $j = 0, 1$ . Therefore, the terms  $\varphi_j(-i), j = 0, 1$  in equation (11)–(12) are the exponential compensators of  $J_j(t)$  required to ensure, together with Assumption 1, that the discounted stock price process is a martingale under the chosen risk neutral probability measure  $\mathbb{P}$ . The independence of  $L_0$  and  $L_1$  is required for the application of the leverage-neutral measure. Further, in equations (9)–(10),  $Z_1(t)$  is a standard Brownian motion and  $\tilde{J}_j(t), j = 0, 1$  are independent (non-positive) pure jump Lévy processes with characteristic exponent  $\varphi_{\tilde{J}_j}(u)$ , and triplet  $\partial\Pi(\tilde{J}_j|\mathbb{P}) = (\tilde{\alpha}_j, 0, \tilde{\nu}_j(dx))$ ,  $j = 0, 1$ .

Thus,  $X(t)$  is formed by two independent Lévy processes, one of which is time changed by a stochastic clock  $T(t)$  governed by the activity rate  $v(t)$ . The same structure is adopted for the process  $v(t)$ . The coefficients  $\sigma_{1,D}, \sigma_{j,J}$ , for  $j = 0, 1$ , capture the proportional scale on the risk processes movements. The model also allows for mean reversion, controlled by the positive parameters  $\kappa, \theta$ , reflecting the empirical observation that the volatility changes associated with stock returns appear to smooth out quickly.

Dependence between the log-returns process and the activity rate is assumed to originate from both diffusion and jump part. Thus,  $Z_1, W_1$  are correlated Brownian motions, so that  $\langle Z_1, W_1 \rangle(t) = \rho t$ ,  $\rho \in [-1, 1]$ ; dependence between the jump parts of  $X(t)$  and  $v(t)$  is induced by a factor construction based on which the corresponding risk sources are decomposed in their systematic and idiosyncratic components. This choice is mainly motivated by the construction parsimony and flexibility as it only requires the characteristic function in explicit form. Factor

constructions for multivariate Lévy processes have been explored by Ballotta and Bonfiglioli (2014), Ballotta et al. (2017, 2019) amongst others.

For this purpose, we distinguish between the positive and negative jumps of the process  $J_j(t)$ , so that  $J_j(t) = J_{j,+}(t) + J_{j,-}(t)$ ,  $\varphi_{J_j}(u) = \varphi_{J_{j,+}}(u) + \varphi_{J_{j,-}}(u)$  and  $\partial\Pi(J_j|\mathbb{P}) = (\alpha_j = \alpha_{j,+} + \alpha_{j,-}, 0, \nu_j(dx) = \nu_{j,+}(dx) + \nu_{j,-}(dx))$ ,  $j = 0, 1$ . As the instantaneous activity rate of the clock is required to be a positive process, and the correlation between the processes of the log-returns and their volatility is usually negative, we identify the process of the negative jumps  $J_{j,-}(t)$ ,  $j = 0, 1$  as the systematic risk component and, after suitable rescaling, we choose it as the risk driver of the jumps of  $v(t)$ , i.e.  $\tilde{J}_j(t) = J_{j,-}(t)$ ,  $j = 0, 1$ . This ensures that the log-returns and the activity rate might jump together: the covariance between the jump processes driving the log-returns and the activity process is in fact governed by the systematic source of risk  $J_{j,-}(t)$ ,  $j = 0, 1$ . Detailed expressions for the covariance depend on the parameters choice, in a sense discussed in Section 3.1.2. Note that in the interest of model parsimony, we assume zero idiosyncratic part in the activity rate process, but the framework could be easily extended to cater for this additional risk process.

Therefore, the proposed construction focuses on dependence effects between log-returns and volatility originated by ‘bad news’ (negative jumps), and reflects the observed empirical regularities that negative returns have a stronger impact on volatilities, whilst positive returns usually show a much weaker effect, or none at all.

We conclude by considering the variance  $V(t)$ , the (squared) volatility of volatility  $q(t)$  and the leverage  $C(t)$ : it follows from equations (3)–(5) that

$$V(t) = \gamma_0 + \gamma_1 v(t), \quad (14)$$

$$q(t) = \gamma_1^2 (\eta_{1,D}^2 v(t) + q_J(t)), \quad (15)$$

$$C(t) = \gamma_1 (\sigma_{1,D} \eta_{1,D} \rho v(t) + C_J(t)), \quad (16)$$

with  $q_J(t)$ ,  $C_J(t)$  denoting respectively the volatility of volatility and ‘instantaneous’ covariance of the jump parts of  $v(t)$  and  $X(t)$ , and  $\gamma_j = \sigma_{j,D}^2 + \sigma_{j,J}^2 \text{Var}(J_j(1))$  denoting the instantaneous variance of the Lévy processes  $L_j(t)$ ,  $j = 0, 1$  (see Appendix A for full details).

The above expressions show that the process  $L_0(t)$  contributes to the current level of the processes of (squared) volatility by means of the level of its instantaneous variance; however, it plays no role in the corresponding dynamics. Moreover, specific expressions for  $q_J(t)$  and  $C_J(t)$  depend on the specific construction of the jumps of  $X(t)$  and  $v(t)$ ; a few examples are discussed in the following Section.

### 3.1.2 Choosing the driving jump process: two-sided tempered stable processes

Although in theory  $J_j(t)$  could be any Lévy process of choice, particular mathematical tractability and modelling flexibility are offered by the class of two-sided tempered stable processes, with Lévy measure

$$\nu(dx) = \left( C_+ \frac{t_+(x)}{x^{1+Y_+}} 1_{x>0} + C_- \frac{t_-(x)}{|x|^{1+Y_-}} 1_{x<0} \right) dx, \quad Y_{\pm} < 2.$$

In other words, this is obtained by multiplying the Lévy measure of a stable process by a function  $t_{\pm}(x)$  whose scope is to temper the large jumps of the process, ensuring finite (high order)

moments, while retaining flexibility of the ‘fine structure’ of the small jumps, controlled by the parameters  $Y_{\pm}$ .

In some more detail, mathematical tractability arises from the immediate identification of the processes of the positive and negative jumps. Flexibility of the ‘fine structure’ arises from the parameters  $Y_{\pm}$ : for  $Y_{\pm} < 0$  the process exhibits a finite number of jumps in any finite time period (i.e. finite activity) and its behaviour is the one typical of a compound Poisson process; for  $Y_{\pm} \in (0, 1)$  the process has trajectories of infinite activity and finite variation, so that relative calmness is observed between big jumps. Finally for  $Y_{\pm} \in (1, 2)$  the process shows a high degree of activity near zero as many small oscillations are observed between big jumps (i.e. infinite variation).

The class of two-sided tempered stable processes encompasses a large number of processes used in the literature, according to the choice of the tempering function  $t_{\pm}(x)$ . We recover the CGMY process of Carr et al. (2002) in correspondence of an exponential tempering and  $C_+ = C_-$ ,  $Y_+ = Y_-$ , with the Variance Gamma process of Madan et al. (1998) a limiting case for  $Y \rightarrow 0$ . The Modified Tempered Stable process follows by tempering with a modified Bessel function of the second kind, whilst the Rapidly Decreasing Tempered Stable process is obtained by adopting a Gaussian tempering function (for full details, we refer to Fallahgoul and Loeper, 2019, and references therein).

The market model summarized in the system (7)–(8) includes as a special case for  $\sigma_{\cdot,J} = \eta_{\cdot,J} = 0$  the Heston (1993) model, in virtue of the Dambis, Dubins-Schwarz theorem (see Revuz and Yor, 1991, for example). Other particular constructions of interest which can be obtained out of the system (7)–(8) are the pure jump versions of both the Heston (1993) (henceforth JH) and the Barndorff-Nielsen and Shephard (2003) (JBNS) model which are novel to the literature and analysed in the following. For ease of exposition, we summarize the detailed specification of all the discussed models in Table 1.

**JH and 1SVFSE models.** Let us set  $\sigma_{0,J} = \sigma_{1,D} = 0$ ,  $\eta_{0,J} = \eta_{1,D} = 0$  and  $\tilde{J}_1(t) = J_{1,-}(t)$  (so that  $\varphi_{\tilde{J}_1}(u) = \varphi_{J_{1,-}}(u)$ ); the activity rate process  $v(t)$  is then driven by the process of the negative jumps of  $L_1(t)$  time changed by the stochastic clock  $T(t)$ , i.e.

$$\begin{aligned} dv(t) &= \kappa(\theta - v(t))dt - \eta_{1,J}dJ_{1,-}(T(t)), \\ dX(t) &= -(\varphi_{1,+}(-i\sigma_{1,J}) + \varphi_{1,-}(-i\sigma_{1,J}))v(t)dt + \sigma_{1,J}dJ_1(T(t)). \end{aligned}$$

This specification can be interpreted as the pure jump analogue of the Heston model due to its construction and the self-exciting nature of the model (see, for example Carr and Wu, 2017, and references therein), as the occurring of a downside movement in the log-return process simultaneously affects the intensity of future downside events and their variance.

Table 1.B shows that the JH model presents stochastic (squared) volatility, volatility of volatility and covariance processes; these are all driven by the activity rate process  $v(t)$ . The correlation process  $\rho(t) = C(t)/\sqrt{V(t)q(t)}$  though is constant, due to the multiplicative nature of the quantities involved in its definition. These features are also shared by the classic Heston model (the only difference being that the processes in question are all pure diffusion).

Further, as  $\langle J_{1,-}, J_1 \rangle(t) = \text{Var}(J_{1,-})t$ , the sign of the leverage effect, i.e. the sign of the covariance process, is controlled by the parameter  $\sigma_{1,J}$ , i.e. the rescaling applied to the time

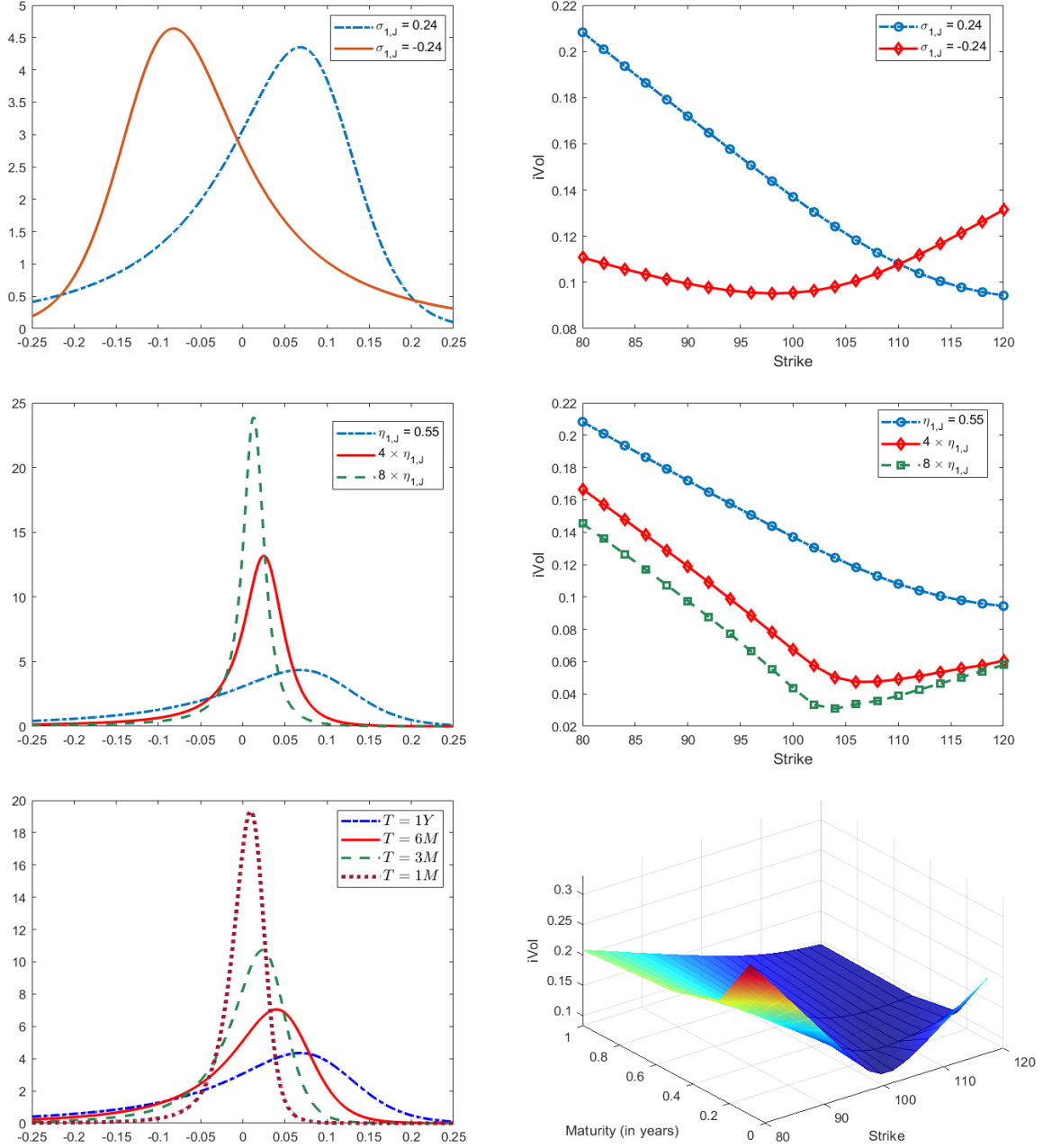


Figure 1: JH model: impact of parameters  $(\sigma_{1,J}, \eta_{1,J})$  and time to maturity ( $T$ : 1 year, 6 months, 3 months, 1 months) on log-returns distribution skewness and excess kurtosis (left hand side panels) and implied volatility (right hand side panels). Base process: CGMY. Test parameters:  $S(0) = 100$ ;  $v(0) = 0.06$ ;  $\kappa = 0.14$ ;  $\theta = 1.97$ ;  $\eta_{1,J} = 0.55$ ;  $\sigma_{1,J} = 0.24$ ;  $C = 1.07$ ;  $G = 0.38$ ;  $M = 6.85$ ;  $Y = 1.56$ ;  $T = 1$ .

changed jump process in the process  $X(t)$ . Figure 1 shows in the top two left-hand side panels the role of the parameters  $\sigma_{1,J}$  and  $\eta_{1,J}$  in controlling the skewness and the excess kurtosis of the log-returns distribution. When ‘translated’ in terms of option implied volatility, we notice in the top two right-hand side panels the link between the sign of the distribution skewness and the slope of the volatility smile/smirk - negative skewness corresponding to a volatility smirk (reverse skew), positive skewness corresponding instead to a volatility forward skew - and the level of excess kurtosis and curvature/convexity of the volatility smirk. This is consistent with the intuition from the approximation formula of Backus et al. (2004). The bottom two panels, instead, focus on the behaviour of both the log-returns distribution and the resulting implied

$v(t) = v(0) + Y_0(t) + Y_1(T(t))$ $X(t) = L_0(t) + L_1(T(t))$	or (equivalently) or (equivalently)	$dv(t) = dY_0(t) + dY_1(T(t))$ $dX(t) = dL_0(t) + dL_1(T(t))$		
<hr/>				
PANEL A - Parameter Specification	Model	Stochastic Differential Equation		
$\eta_{0,J} = \eta_{1,D} = 0$ $\sigma_{0,J} = \sigma_{1,D} = 0$	Pure Jump Heston (JH)	$dv(t) = \kappa(\theta - v(t))dt - \eta_{1,J}dJ_{1,-}(T(t))$ $dX(t) = -(\varphi_{1,+}(-i\sigma_{1,J}) + \varphi_{1,-}(-i\sigma_{1,J}))v(t)dt + \sigma_{1,J}dJ_1(T(t))$		
$\eta_{1,J} = \eta_{1,D} = 0$ $\sigma_{0,J} = \sigma_{1,D} = 0$	Pure Jump BNS (JBNS)	$dv(t) = \kappa(\theta - v(t))dt - \eta_{0,J}dJ_{1,-}(t)$ $dX(t) = -(\varphi_{1,+}(-i\sigma_{1,J}) + \varphi_{1,-}(-i\sigma_{1,J}))v(t)dt + \sigma_{1,J}dJ_1(T(t))$		
$\eta_{0,J} = \eta_{1,J} = 0$ $\sigma_{l,J} = 0, l = 0, 1$	Heston (Heston, 1993)	$dv(t) = \kappa(\theta - v(t))dt + \eta_{1,D}\sqrt{v(t)}dZ_1(t)$ $dX(t) = -\sigma_{1,D}^2v(t)/2dt + \sigma_{1,D}\sqrt{v(t)}dW_1(t)$		
$\eta_{0,J} = 0$ $\sigma_{0,J} = 0$	1 Factor Self-Exciting (1SVFSE)	$dv(t) = \kappa(\theta - v(t))dt + \eta_{1,D}\sqrt{v(t)}dZ_1(t) - \eta_{1,J}dJ_{1,-}(T(t))$ $dX(t) = -\left(\sigma_{1,D}^2/2 + \varphi_{1,+}(-i\sigma_{1,J}) + \varphi_{1,-}(-i\sigma_{1,J})\right)v(t)dt + \sigma_{1,D}\sqrt{v(t)}dW_1(t) + \sigma_{1,J}dJ_1(T(t))$		
$\eta_{1,J} = 0$ $\sigma_{0,J} = 0$	1 Factor Heston + OU (1SVFHOU)	$dv(t) = \kappa(\theta - v(t))dt + \eta_{1,D}\sqrt{v(t)}dZ_1(t) - \eta_{0,J}dJ_{1,-}(t)$ $dX(t) = -\left(\sigma_{1,D}^2/2 + \varphi_{1,+}(-i\sigma_{1,J}) + \varphi_{1,-}(-i\sigma_{1,J})\right)v(t)dt + \sigma_{1,D}\sqrt{v(t)}dW(t) + \sigma_{1,J}dJ_1(T(t))$		
<hr/>				
PANEL B - Parameter Specification	Model	$V(t)$	$q(t)$	$C(t)$
$\eta_{0,J} = \eta_{1,D} = 0$ $\sigma_{0,J} = \sigma_{1,D} = 0$	JH	$\sigma_{1,J}^2\mathbb{V}ar(J_1(1))v(t)$	$\sigma_{1,J}^4\eta_{1,J}^2\mathbb{V}ar(J_1(1))^2\mathbb{V}ar(J_{1,-}(1))v(t)$	$-\sigma_{1,J}^3\eta_{1,J}\mathbb{V}ar(J_1(1))\mathbb{V}ar(J_{1,-}(1))v(t)$
$\eta_{1,D} = \eta_{1,J} = 0$ $\sigma_{0,J} = \sigma_{1,D} = 0$	JBNS	$\sigma_{1,J}^2\mathbb{V}ar(J_1(1))v(t)$	$\sigma_{1,J}^4\eta_{0,J}^2\mathbb{V}ar(J_1(1))^2\mathbb{V}ar(J_{1,-}(1))$	$-\sigma_{1,J}^3\eta_{0,J}\mathbb{V}ar(J_1(1))\mathbb{V}ar(J_{1,-}(1))(1+v(t))$
$\eta_{0,J} = \eta_{1,J} = 0$ $\sigma_{l,J} = 0, l = 0, 1$	Heston	$\sigma_{1,D}^2v(t)$	$\sigma_{1,D}^4\eta_{1,D}^2v(t)$	$\sigma_{1,D}^3\eta_{1,D}\rho v(t)$
$\eta_{0,J} = 0$ $\sigma_{0,J} = 0$	1SVFSE	$\gamma_1v(t)$	$\gamma_1^2\left(\eta_{1,D}^2 + \eta_{1,J}^2\mathbb{V}ar(J_{1,-}(1))\right)v(t)$	$\gamma_1(\sigma_{1,D}\eta_{1,D}\rho - \sigma_{1,J}\eta_{1,J}\mathbb{V}ar(J_{1,-}(1)))v(t)$
$\eta_{1,J} = 0$ $\sigma_{0,J} = 0$	1SVFHOU	$\gamma_1v(t)$	$\gamma_1^2\left(\eta_{1,D}^2v(t) + \eta_{0,J}^2\mathbb{V}ar(J_{1,-}(1))\right)$	$\gamma_1(\sigma_{1,D}\eta_{1,D}\rho v(t) - \sigma_{1,J}\eta_{0,J}\mathbb{V}ar(J_{1,-}(1))(1+v(t)))$

Table 1: Panel A: Under each class of parameter configurations, entries summarize the Stochastic Volatility model specifications nested in the setup given by equations (7)–(8). Panel B: Main features of the corresponding Stochastic Volatility model specifications. Features: squared volatility process,  $V(t)$ , squared volatility of volatility process,  $q(t)$ , ‘instantaneous covariance’ process,  $C(t)$  - see Section 3.1. Note:  $\eta_{1,D} \geq 0, \eta_{j,J} \geq 0, \sigma_{j,D} \geq 0, \sigma_{i,J} \in \mathbb{R}$  for  $j = 0, 1$ ; finally  $\langle W_1, Z_1 \rangle(t) = \rho t$ ,  $\rho \in [-1, 1]$ .  $\gamma_1 = \sigma_{1,D}^2 + \sigma_{1,J}^2\mathbb{V}ar(J_1(1))$ . Proof of results in Panel B: see Appendix A.

volatility surface over different time horizons. For short time periods, corresponding to short maturity contracts, the JH distribution is strongly skewed and leptokurtic, which translates in a very convex implied volatility (see the steepness of the curve around the at-the-money - ATM - strike). Skewness and excess kurtosis tend to fade over longer periods of time, which causes the volatility surfaces to flatten out for longer dated contracts.

The patterns observed in Figure 1 are consistent with the empirical evidence reported by, amongst other, Gatheral (2006) and Ait-Sahalia et al. (2021); this shows the ability of the JH model to reproduce realistic volatility patterns.

A more general specification retaining the self-exciting structure described above can be obtained by ‘switching back on’ the diffusion components of both processes  $(v(t), X(t))$ , i.e. allowing for  $\eta_{1,D}, \sigma_{1,D} > 0$ . We term this specification the one stochastic volatility factor self-exciting (1SVFSE) model, due to the link between the changes in the log-return process and the intensity of future changes and their variance, which are originated in this case by both the continuous and discontinuous parts of the risk driver. The Heston and JH models can then be recovered as special cases by suitable setting of the parameters. The role of the parameters is shown in Figure 2, in which we specifically focus on  $\rho$  and  $\eta_{1,D}$  and their impact respectively on the sign of the skewness and the level of the excess kurtosis (top two panels on the left-hand side), as in the classical Heston model, and the corresponding effect on the smirk/smile shape of the implied volatility curve (top two panels on the right-hand side). In addition, we also study the impact of  $\sigma_{1,J}$  and  $\eta_{1,J}$ : Figure 2 shows that the discontinuous part of the dynamics - controlled by these parameters - offers increased flexibility in fitting the shape of the implied volatility. The model is also capable of producing steep slopes of the ATM volatility, as shown in the bottom panels of Figure 2; however such steepness, as well as the excess kurtosis of the log-returns distribution tend to persist even for longer maturities.

**JBNS and 1SVFHOU models.** By setting  $\sigma_{0,J} = \sigma_{1,D} = 0$ ,  $\eta_{1,J} = \eta_{1,D} = 0$  and  $\tilde{J}_0(t) = J_{1,-}(t)$  (so that  $\varphi_{\tilde{J}_0}(u) = \varphi_{J_{1,-}}(u)$ ) we obtain the pure jump analogue of the BNS model, although leverage is in this case originated by the dependence between the base process of  $X(t)$  and the background driving Lévy process (BDLP) of the activity rate. The system, in fact, reads

$$\begin{aligned} dv(t) &= \kappa(\theta - v(t))dt - \eta_{0,J}dJ_{1,-}(t), \\ dX(t) &= -(\varphi_{1,+}(-i\sigma_{1,J}) + \varphi_{1,-}(-i\sigma_{1,J}))v(t)dt + \sigma_{1,J}dJ_1(T(t)). \end{aligned}$$

Indeed the activity rate follows a mean-reverting non-Gaussian Ornstein-Uhlenbeck (OU) process as in Barndorff-Nielsen and Shephard (2003), with  $J_{1,-}(t)$  as BDLP. Thus, volatility suddenly jumps up due to a (negative) jump in the asset log-return process and calms down afterwards with exponential decay. From Table 1.B, we observe that the JBNS model is characterised by constant squared volatility of volatility, as expected as the increments of the corresponding conditional variance are independent and stationary. The correlation coefficient, though, is stochastic. As  $\langle J_{1,-}, J_1 \rangle(t) = \text{Var}(J_{1,-})t$  also for this model, the parameters  $\sigma_{1,J}$  and  $\eta_{0,J}$  play a similar role as  $\sigma_{1,J}$  and  $\eta_{1,J}$  in the JH model (results available upon request).

Similarly to the case above, we can generate a more general one stochastic volatility factor version for this modified BNS model by letting  $\eta_{1,D}, \sigma_{1,D} > 0$ ; we term this specification one stochastic volatility factor Heston-OU (1SVFHOU) model. This construction retains randomness

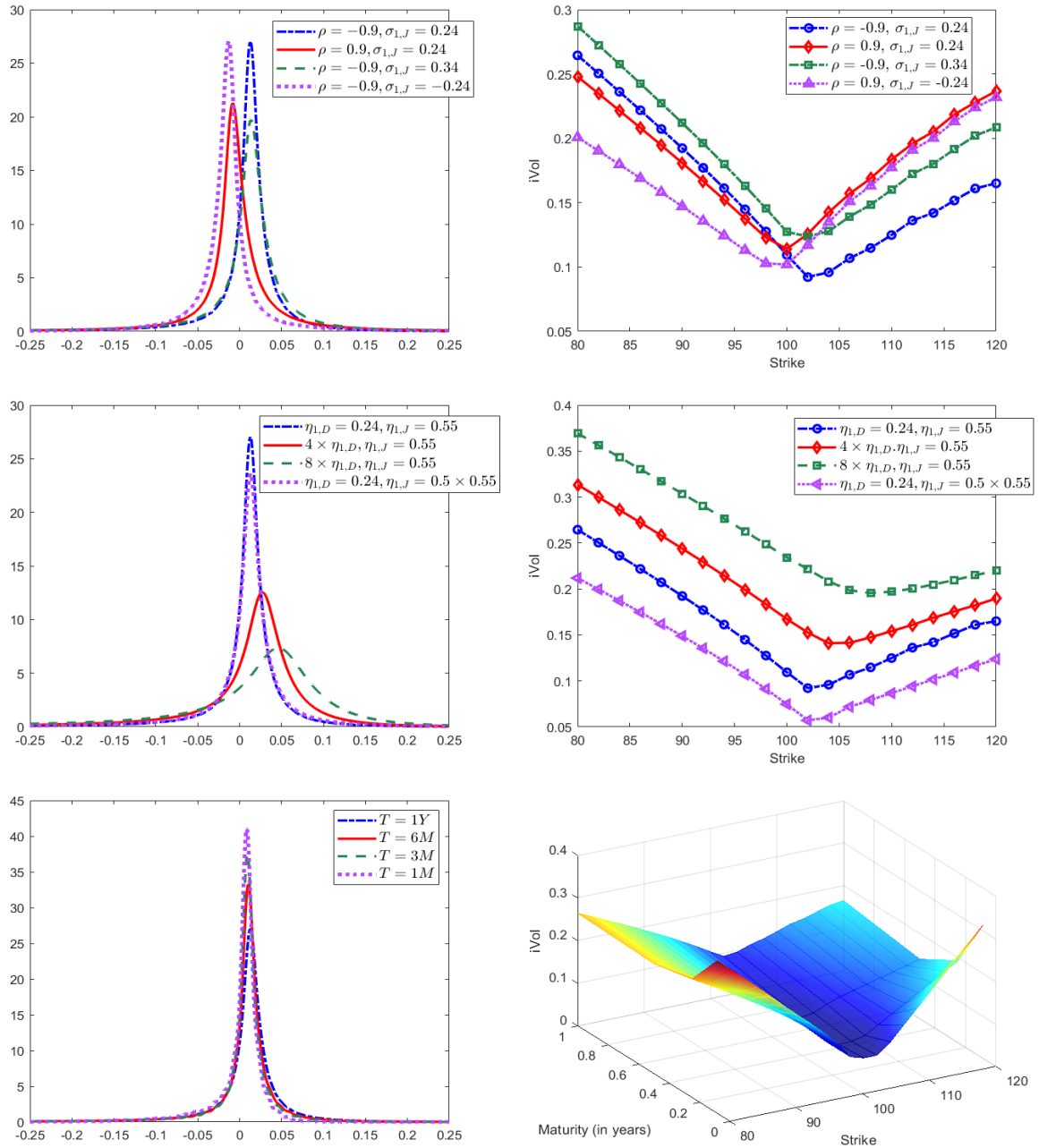


Figure 2: 1SVFSE model: impact of parameters  $(\rho, \eta_{1,D})$ ,  $(\sigma_{1,J}, \eta_{1,J})$  and time to maturity ( $T$ : 1 year, 6 months, 3 months, 1 months) on log-returns distribution skewness and excess kurtosis (top panels) and implied volatility (bottom panels). Base process: CGMY. Test parameters:  $S(0) = 100$ ;  $v(0) = 0.06$ ;  $\kappa = 0.14$ ;  $\theta = 1.97$ ;  $\eta_{1,D} = 0.24$ ;  $\rho = -0.9$ ;  $\sigma_{1,D} = 0.28$ ;  $\eta_{1,J} = 0.55$ ;  $\sigma_{1,J} = 0.24$ ;  $C = 1.07$ ;  $G = 0.38$ ;  $M = 6.85$ ;  $Y = 0.8$ ;  $T = 1$ .

in both the squared volatility of volatility and correlation process, due to the superposition of the square root process and the OU process in the activity rate - see Table 1.B.

This analysis also shows that, contrary to common belief, one stochastic volatility factor models can indeed generate stochastic correlation as long as jumps are included in the relevant dynamics, and are not generated exclusively by means of TCLP.

Finally, a large number of models proposed in the option pricing literature can be rewritten in terms of the specification given in (7)–(8) by suitably setting the model parameters and jump structure. Other specifications that can be recovered by our setting include for example the ones of Barndorff-Nielsen and Shephard (2003), Bates (1996), Eraker et al. (2003), Eraker (2004), Pan

(2002), Carr et al. (2003), the SV1 and SV3 specifications of Huang and Wu (2004), and the models encompassed by Coqueret and Tavin (2016) amongst others.

### 3.2 Characteristic function

As mentioned in Section 2, we obtain the characteristic function of the log-returns process by means of the leverage-neutral measure introduced by Carr and Wu (2004). For the specific case of the framework set out in Section 3.1, the leverage-neutral measure  $\mathbb{M}$  is defined by the complex-valued exponential martingale

$$M_u(t) = e^{iuL_0(t) - \varphi_{L_0}(u)t + iuL_1(T(t)) - \varphi_{L_1}(u)T(t)}; \quad (17)$$

consequently, the characteristic function of  $X(t)$  reads

$$\phi_X(u; t) = \phi_T^{\mathbb{M}}(-i\varphi_{L_1}(u); t) e^{\varphi_{L_0}(u)t}. \quad (18)$$

Useful mathematical expressions for equation (18) can be recovered once the characteristic function of the integrated process is specified. To this purpose, though, we need first to recover the dynamics of the process  $v(t)$  under the new measure  $\mathbb{M}$ , which follows from the  $\mathbb{M}$ -dynamics of the log-return process  $X(t)$  in virtue of the dependence in place. As observed in Section 2, it suffices to recover the dynamics of the base process  $L_j(t)$ ,  $j = 0, 1$ , as given in the following.

**Proposition 1** *Consider the model setup given in equations (7)–(8) and the leverage neutral measure  $\mathbb{M}$  defined by the process  $M_u(t)$  given in (17). Then.*

*i)  $W_1(t) - iu\sigma_{1,D}t$  is a  $\mathbb{M}$ -Brownian motion; the pure jump processes driving the base of the log-returns have characteristic exponent  $\varphi_{J_{j,-}}^{\mathbb{M}}(z) + \varphi_{J_{j,+}}^{\mathbb{M}}(z)$ ,  $j = 0, 1$ , both satisfying equation (6).*

*ii)  $Z_1^{\mathbb{M}}(t) = Z_1(t) - iu\sigma_{1,D}pt$  is a  $\mathbb{M}$  Brownian motion; the pure jump Lévy processes driving the activity rate under  $\mathbb{M}$ ,  $\tilde{J}_j^{\mathbb{M}}(t)$ ,  $j = 0, 1$ , have characteristic exponent satisfying the relationship*

$$\varphi_{\tilde{J}_j}^{\mathbb{M},u}(z) = \varphi_{\tilde{J}_j}(z + \sigma_{l,J}u) - \varphi_{\tilde{J}_j}(\sigma_{l,J}u), \quad j, l = 0, 1. \quad (19)$$

The coefficient  $\sigma_{.,J}$  detects the part of the base process which  $\tilde{J}_j(t)$ ,  $j = 0, 1$ , shares a systematic component with.

Thus, under the  $\mathbb{M}$ -measure

$$v(t) = v(0) + Y_0^{\mathbb{M}}(t) + Y_1^{\mathbb{M}}(T(t))$$

for

$$\begin{aligned} dY_0^{\mathbb{M}}(t) &= \kappa\theta dt - \eta_{0,J}d\tilde{J}_0^{\mathbb{M}}(t) \\ dY_1^{\mathbb{M}}(t) &= -\kappa^{\mathbb{M}}dt + \eta_{1,D}dZ_1^{\mathbb{M}}(t) - \eta_{1,J}d\tilde{J}_1^{\mathbb{M}}(t); \end{aligned}$$

with  $\kappa^{\mathbb{M}} = \kappa - iu\eta_{1,D}\sigma_{1,D}\rho$ . Due to the affine structure of the model, the following holds.

**Proposition 2** Consider the model setup given in equations (7)–(8). Then the process  $X(t)$  admits characteristic function

$$\phi_X(u; t) = e^{A(t)+B(t)v(0)},$$

with the affine exponents  $A, B$  solutions to the system of Riccati-type ODEs

$$\begin{aligned} A'(t) &= \varphi_{L_0}(u) + \kappa\theta B(t) + \varphi_{\bar{j}_0}^{\mathbb{M}}(i\eta_{0,J}B(t)), \\ A(0) &= 0 \end{aligned} \tag{20}$$

$$\begin{aligned} B'(t) &= \varphi_{L_1}(u) - \kappa^{\mathbb{M}}B(t) + \frac{\eta_{1,D}^2}{2}B(t) + \varphi_{\bar{j}_1}^{\mathbb{M}}(i\eta_{1,J}B(t)), \\ B(0) &= 0. \end{aligned} \tag{21}$$

The set up under consideration also gives access to the forward characteristic function, which is necessary for pricing forward volatility/skew dependent contracts, such as forward start options. The result is offered in the following.

**Proposition 3** Consider the model setup given in equations (7)–(8). Then the process  $X(t)$  admits forward characteristic function

$$\phi_X(u; s, t) = \mathbb{E}\left(e^{X(t)-X(s)}\right) = e^{A(t-s)+C(s)+D(s)v(0)}, \quad s \leq t,$$

with the affine exponents  $C, D$  solutions to the system of Riccati-type ODEs

$$\begin{aligned} C'(s) &= \kappa\theta D(s) + \varphi_{\bar{j}_0}(i\eta_{0,J}D(s)), \\ C(0) &= 0 \end{aligned} \tag{22}$$

$$\begin{aligned} D'(s) &= -\kappa D(s) + \frac{\eta_{1,D}^2}{2}D(s) + \varphi_{\bar{j}_1}(i\eta_{1,J}D(s)), \\ D(0) &= B(t-s). \end{aligned} \tag{23}$$

and  $A(t-s), B(t-s)$  as in Proposition 2.

The affine exponents in Propositions 2 and 3 can be obtained in closed-form in specific cases depending on the choice of the Lévy process of reference, the most notable of which is the classical Heston model. For the model specifications introduced in this paper, the characteristic function of the JH model can only be recovered numerically using the standard Runge-Kutta 4th-order method; similar considerations hold for the 1SVFSE. In the case of the JBNS and 1SVFHO models instead semi-analytical solutions can be obtained (up to numerical integration). All the relevant characteristic functions are reported in Table 2.

### 3.3 Enlarging the market model: two Stochastic Volatility Factors

Existing contributions in the literature (see Christoffersen et al., 2009, for example) highlight that the shape of the smile is largely independent of the current volatility level, as data show the presence of days with low volatility and both steep and flat volatility slopes (and viceversa). However, they argue that one SV factor models such as the ones discussed so far are not flexible enough in modelling this relationship between the volatility level and the slope of the smile. The standard solution proposed in the literature is to augment the model with multiple stochastic

Model	$\phi_X(u; t) = e^{A(t)+B(t)v(0)}$ $A(t)$	$B(t)$	$\phi_X(u; s, t) = e^{A(t-s)+C(s)+D(s)v(0)}, s \leq t$ $C(s)$	$D(s)$
JH	Numerically solve $A'(t) = \kappa\theta B(t), A(0) = 0$ $B'(t) = \varphi_{L_1}(u) - \kappa B(t) + \varphi_{J_1,-}^M(i\eta_{1,J}B(t)), B(0) = 0$		Numerically solve $C'(s) = \kappa\theta D(s), C(0) = 0$ $D'(s) = -\kappa D(s) + \varphi_{J_1,-}(i\eta_{1,J}D(s)), D(0) = B(t-s)$	
JBNS	$\varphi_{L_1}(u)\theta(t - \varepsilon(\kappa; t)) + \int_0^t \varphi_{J_0,-}^M(i\eta_{0,J}B(s)) ds$ $\varepsilon(\kappa; t) = (1 - e^{-\kappa t}) / \kappa$	$\varphi_{L_1}(u)\varepsilon(\kappa; t)$	$\theta B(t-s)(1 - e^{-\kappa s}) + \int_0^s \varphi_{J_0,-}(i\eta_{0,J}D(s)) ds$	$B(t-s)e^{-\kappa s}$
Heston	$\frac{\kappa\theta}{\eta_{1,D}^2} \left( (\kappa^M - d)t - 2 \ln \frac{1 - ge^{-dt}}{1-g} \right)$ $d = \sqrt{(\kappa^M)^2 - 2\eta_{1,D}^2 \varphi_{L_1}(u)}$ $\kappa^M = \kappa - iu\eta_{1,D}\sigma_{1,D}\rho$	$\frac{\kappa^M - d}{\eta_{1,D}^2} \frac{1 - e^{-dt}}{1 - ge^{-dt}}$ $g = \frac{\kappa^M - d}{\kappa^M + d}$	$-\frac{2\kappa\theta}{\eta_{1,D}^2} \ln \left( 1 - B(t-s) \frac{\eta_{1,D}^2}{2\kappa} (1 - e^{-\kappa s}) \right)$	$\frac{B(t-s)e^{-\kappa s}}{1 - B(t-s) \frac{\eta_{1,D}^2}{2\kappa} (1 - e^{-\kappa s})}$
ISVFSE	Numerically solve $A'(t) = \kappa\theta B(t), A(0) = 0$ $B'(t) = \varphi_{L_1}(u) - \kappa^M B(t) + \frac{\eta_{1,D}^2}{2} B^2(t) + \varphi_{J_1,-}^M(i\eta_{1,J}B(t)), B(0) = 0$ $\kappa^M$ as in the Heston model		Numerically solve $C'(s) = \kappa\theta D(s), C(0) = 0$ $D'(s) = -\kappa D(s) + \frac{\eta_{1,D}^2}{2} D(s) + \varphi_{J_1,-}(i\eta_{1,J}D(s)), D(0) = B(t-s)$	
ISVFHOU	$\frac{\kappa\theta}{\eta_{1,D}^2} \left( (\kappa^M - d)t - 2 \ln \frac{1 - ge^{-dt}}{1-g} \right) + \int_0^t \varphi_{J_0,-}^M(i\eta_{0,J}B(s)) ds$ $d, g, \kappa^M$ as in the Heston model	$\frac{\kappa^M - d}{\eta_{1,D}^2} \frac{1 - e^{-dt}}{1 - ge^{-dt}}$	$-\frac{2\kappa\theta}{\eta_{1,D}^2} \ln \left( 1 - B(t-s) \frac{\eta_{1,D}^2}{2\kappa} (1 - e^{-\kappa s}) \right) + \int_0^s \varphi_{J_0,-}(i\eta_{0,J}D(s)) ds$	$\frac{B(t-s)e^{-\kappa s}}{1 - B(t-s) \frac{\eta_{1,D}^2}{2\kappa} (1 - e^{-\kappa s})}$

Table 2: Affine exponents defining the characteristic function and the forward characteristic function of  $X(t)$  (Propositions 2-3).  $\varphi_{L_1}(u)$  as in Equation (13).

volatility factors, see for example Christoffersen et al. (2009), Pun et al. (2015) and Andersen et al. (2015) amongst other. In light of this argument, in the remainder of this section we explore how our setup can be adapted to accommodate a two factor model construction.

To this purpose, the log-return driving process is now simplified to  $X(t) = L_1(T(t))$ . Further, let us re-write the base Lévy process as

$$\begin{aligned}
L_1(t) &= \underbrace{-\frac{\sigma_{1,D}^2}{2}t + \sigma_{1,D}W_1(t)}_{L_{1,D}(t)} \underbrace{-\varphi_{1,+}(-i\sigma_{1,J}) - \varphi_{1,-}(-i\sigma_{1,J})t + \sigma_{1,J}J_1(t)}_{L_{1,J}(t)}, \quad \sigma_{1,D} > 0, \sigma_{1,J} \in \mathbb{R} \\
&= L_{1,D}(t) + L_{1,J}(t).
\end{aligned}$$

In order to incorporate more than one stochastic volatility factor, we decouple the clocks due to the orthogonality of diffusion and jump processes, and we apply separate clocks to the diffusion part,  $L_{1,D}(t)$ , and the jump process,  $L_{1,J}(t)$ . Thus, let us define two random clocks  $T_D(t) = \int_0^t v_D(s)ds$  and  $T_J(t) = \int_0^t v_J(s)ds$  with activity rates

$$\begin{aligned}
v_D(t) &= v_D(0) + Y_{0,D}(t) + Y_{1,D}(T_D(t)) \\
v_J(t) &= v_J(0) + Y_{0,J}(t) + Y_{1,J}(T_J(t)),
\end{aligned}$$

for

$$\begin{aligned}
dY_{0,D}(t) &= \kappa_D\theta_D dt, & dY_{1,D}(t) &= -\kappa_D dt + \eta_{1,D}dZ_1(t), \\
dY_{0,J}(t) &= \kappa_J\theta_J dt - \eta_{0,J}d\tilde{J}_0(t), & dY_{1,J}(t) &= -\kappa_J dt - \eta_{1,J}d\tilde{J}_1(t), \\
\eta_{1,D}, \eta_{0,J}, \eta_{1,J} &\geq 0.
\end{aligned}$$

Then, we set the driver of the log-return process as  $X(t) = L_{1,D}(T_D(t)) + L_{1,J}(T_J(t))$ .

We observe the similarity between the proposed construction and the double Heston SV model of Christoffersen et al. (2009): the variance is now the sum of two independent factors that may be individually correlated with stock returns. Indeed

$$\begin{aligned} V(t) &= V_D(t) + V_J(t) \\ q(t) &= q_D(t) + q_J(t) \\ C(t) &= C_D(t) + C_J(t), \end{aligned}$$

i.e. they inherit the two-factor construction. The analytical expressions can then be recovered from the entries in Table 1, according to the chosen parameter settings.

In this setting it is straightforward to obtain the two stochastic volatility factor version of the self-exciting model (2SVFSE) by setting  $\eta_{0,J} = 0$  and  $\tilde{J}_1(t) = J_{1,-}(t)$ ; the two stochastic volatility factor version based on OU jumps (2SVFHOU) is instead obtained by setting  $\eta_{1,J} = 0$  and  $\tilde{J}_0(t) = J_{1,-}(t)$ . The orthogonality between diffusion and jumps also implies that the characteristic function is the product of the characteristic functions of the classic Heston model and the pure jump model

$$\phi_X(u; t) = \mathbb{E} \left( e^{iuL_{1,D}(T_D(t))} \right) \mathbb{E} \left( e^{iuL_{1,J}(T_J(t))} \right);$$

these can be read from the first three entries of Table 2. Similar arguments hold for the forward characteristic function.

Other 2-factor constructions can be obtained out of the given setting, e.g. like the one in Fulop et al. (2014), although they might carry a higher degree of complexity due to the increasing number of ODEs to be simultaneously solved for the recovery of the required characteristic functions.

Further, we note the complexity of the parameter space: each model is described by the 3 ‘fixed’ parameters for each volatility dynamic, i.e. mean reversion, long run mean and initial volatility level, 3 parameters for the diffusion part  $(\sigma_{1,D}, \eta_{1,D}, \rho)$ , to which we add  $2+n$  parameters for the jump part, i.e.  $\sigma_{\cdot,J}, \eta_{\cdot,J}$  and the  $n$  parameters describing the pure jump process adopted for the constructions offered in this paper. Then, the two stochastic volatility factors models are described by  $11 + n$  parameters, whilst the one stochastic volatility factor models are described by  $5 + n$  parameters in the pure jump case (JH, JBNS) and  $8 + n$  parameters in the diffusion and jump case (1SVFSE, 1SVFHOU). Other 2-factor constructions would inevitably come at the cost of further increasing the parameter space.

## 4 Model performance analysis

The aim of this section is to analyse the relative performance of the models introduced in Section 3 in reproducing market option prices as closely as possible. As discussed in the Introduction, this is an essential requirement for a successful hedging strategy based on vanilla options. For illustration purposes, we consider the case of S&P500 options.

### 4.1 The setup

**The base process.** In order to make the modelling concrete, we choose the CGMY process of Carr et al. (2002) as the relevant base Lévy process. The CGMY process is a 4-parameter version

of a two-side tempered stable process with exponential tempering function; the corresponding Lévy measure is

$$\nu(x) = C \left( \frac{e^{-G|x|}}{|x|^{1+Y}} 1_{x<0} + \frac{e^{-Mx}}{x^{1+Y}} 1_{x>0} \right),$$

for  $C > 0$ ,  $G \geq 0$ ,  $M \geq 0$ ,  $Y < 2$ ; the parameters  $G$  and  $M$  control the arrival of negative and positive size jumps respectively, and consequently govern the skewness of the process distribution: the process has positive (resp. negative) skewness if  $G > M$  (resp.  $G < M$ ). Further, the process distribution is leptokurtic and the excess kurtosis is controlled by the parameter  $C$ .

Thus, the characteristic exponents of the processes of the negative and positive jumps of the CGMY are respectively

$$\varphi_-(u) = C\Gamma(-Y) \left( (G + iu)^Y - G^Y \right), \quad \varphi_+(u) = C\Gamma(-Y) \left( (M - iu)^Y - M^Y \right). \quad (24)$$

Calibration to market data would allow us to learn about the structure of the jumps and their frequency via the parameter  $Y$  which, as discussed in Section 3.1, permits to distinguish between low frequency large jumps, and high frequency small jumps.

In the context of the model presented in Section 3.1, the terms defining equations (20)–(21) are

$$\begin{aligned} \varphi_{J_j, -}^{\mathbb{M}}(u) &= C\Gamma(-Y) \left( (G^{\mathbb{M}} + iu)^Y - (G^{\mathbb{M}})^Y \right), \quad j = 0, 1 \\ G^{\mathbb{M}} &= G + iu\sigma_{j,J}, \quad j = 0, 1. \end{aligned} \quad (25)$$

Indeed, Proposition 1 implies that

$$\varphi^{\mathbb{M}}(z) = C\Gamma(-Y) \left( (G^{\mathbb{M}} + iz)^Y - (G^{\mathbb{M}})^Y + (M^{\mathbb{M}} - iz)^Y - (M^{\mathbb{M}})^Y \right)$$

for  $G^{\mathbb{M}} = G + iu\sigma_{\cdot,J}$  and  $M^{\mathbb{M}} = M - iu\sigma_{\cdot,J}$ .

The characteristic function of each model can then be obtained by substitution in the expressions reported in Table 2; finally we convert characteristic functions into option prices via an efficient algorithm for Fourier inversion. We adopt the COS method of Fang and Oosterlee (2008); other available methods are the ones proposed by Eberlein et al. (2010), and more recently by Kirkby (2015), Callegaro et al. (2019) and Cui et al. (2019) amongst others.

**Calibration and the optimization problem.** The vector of the relevant admissible parameters for each model is obtained by a non-linear least squares optimizer which minimizes the total calibration error across all quotes available on each observation date  $t$ . The error is defined as

$$f_t(\Theta, v(t)) = \sum_j \sum_l \left( \frac{C_{mod}(t, K_j, T_l; \Theta, v(t)) - C_{mkt}(t, K_j, T_l)}{\text{Vega}(K_j, T_l)} \right)^2, \quad (26)$$

with  $\Theta$  denoting the model specific parameters and  $v(t)$  the activity rate level at the observation date  $t$  - we note that in the two stochastic volatility factor setting  $v(t)$  would denote the vector  $(v_D(t), v_J(t))$ . Further,  $C_{mod}$ ,  $C_{mkt}$  denote respectively the model and market option prices for each maturity and strike, and Vega is the corresponding Black-Scholes Vega computed using the

Black-Scholes implied volatilities<sup>2</sup>.

The objective function in equation (26) can be considered as an approximation to implied volatility errors due to the rescaling of the option prices by the Vega (see Carr and Wu, 2007, for example). This choice allows us to carry out the calibration procedure in an efficient way mainly for the following two reasons. In the first place, a norm in implied volatility errors rather than prices avoids the introduction of bias due to expensive in-the-money and/or long-dated options. In second place, the rescaling by Vega allows us to bypass the recovery of the implied volatility via Black-Scholes inversion of model prices, which might become very costly numerically. Finally, the level of the activity rate is considered as another unknown to be calibrated from market quotes. We note that as in Huang and Wu (2004), Christoffersen et al. (2009), we use only option prices for the calibration; alternative approaches based on the series of the underlying returns to filter volatility could be used, but are beyond the scope of this paper. We refer to Christoffersen et al. (2009) for further discussions on advantages/disadvantages of this choice.

Further, we observe that in practice the parameters of financial models are usually distinguished as either market parameters, i.e. input reflecting market data and therefore requiring regular updates before pricing and/or executing new deals, or model parameters, i.e. input reflecting modelling choices not necessarily subject to changes following daily market movements. In our setting, the spot price and the spot volatilities at every observation time point represent the market risk to the financial operator, and therefore are the market parameters. As a ‘good’ model should remain market consistent by updating the market parameters only, and the spot volatility is a latent quantity, we perform the calibration through a two step procedure similar to the one adopted in Huang and Wu (2004) and Christoffersen et al. (2009) amongst others, which is organized as follows.

Let  $T$  denote the total number of observation dates in the dataset. In step one we solve the aggregate optimization problem

$$\min_{\Theta, v} \sum_{t=1}^T f_t(\Theta, v), \quad (27)$$

for all contracts in the dataset, and the objective function as in equation (26) with the spot volatility kept constant across all dates at this stage. Let  $\Theta^*$  denote the resulting optimal model parameter set. Then, step two consists of solving the optimization problems

$$\min_{v(t)} f_t(\Theta^*, v(t)), \quad t = 1, \dots, T, \quad (28)$$

i.e., at each observation date  $t$  we choose the spot activity rate (vector)  $v(t)$  as to minimize the calibration error by keeping the model specific parameters fixed to their optimal value.

Due to the choice of objective function, the calibration performance is measured by the implied volatility root mean squared error (IVRMSE).

---

<sup>2</sup>The ratio in (26) is well defined for non-zero Vegas; vanishing Vegas can happen for options with very short maturities and/or low implied volatility. The filters applied to our dataset - see Appendix B - have prevented such instances.

## 4.2 Results

In this section, we assess the performance of the models described in this paper with respect to the performance measures given in the previous section. In order to provide a term of comparison, the benchmark for the calibration performance is the Heston (1993) model, which fits into the general setting of equations (7)–(8). Due to the similarity between our proposed 2 SV factors construction and the double stochastic volatility model of Christoffersen et al. (2009), we consider the latter as well.

The analysis is organized in two calibration exercises. In the first one, we consider the case in which the models are calibrated to the market volatility surface at a specific day, in line with market practice. In the second calibration exercise, we consider a dataset spanning a longer period of time non overlapping with the one used in the previous experiment, with the aim of discussing the reliability of the calibration parameters, by means of a out-of-sample test of results.

**Calibration Exercise 1.** We consider option quotes on the S&P500 observed on April 24th 2017 on the Bloomberg platform; we build the full volatility surface using the SVI methodology of Gatheral and Jacquier (2014) for a total of 1,573 points. The maturities of the option contracts range from 25 to 970 business days; finally, for all maturities we use the same range of moneyness from 0.85 to 1.25 (full details of the dataset in Appendix B).

The calibrated parameters are obtained by solving the optimization problem (27)–(28). The optimal solution and the corresponding performance measures for each model are reported in Table 3 (the breakdown of the IVRMSE generated by each model across maturities and moneyness is reported in Appendix C).

With respect to the benchmark, all models provide a significant improvement in the performance of the calibration across all maturities and level of moneyness, although the largest error reduction occurs for short dated contracts. The best performing models in this respect are the self-exciting structures (JH, 1/2SVFSE) and the 1SVFHOU model; their calibration performance though is very similar.

Thus the implications on model designs are as follows: firstly, the model for the underlying asset needs to allow for randomness not only in the volatility process, but also in the volatility of volatility and the covariance process. Further, the model should have the ability to ‘learn’ from data the fine structure of the jumps, which in our setting is controlled by the value of the  $Y$  parameter. Indeed, both the JH and the 2SVFSE structures show jumps of infinite variation ( $Y > 1$ ). The relatively unsatisfactory performance of the JBNS model seems indeed due to a combination of these features - the calibrated value of the parameter  $Y$  in this model is less than 1, indicating finite variation jumps. However the calibration results do not reveal the presence of (compound) Poisson-type of jumps:  $Y$  is always positive denoting infinite activity.

Finally, in the case of the self-exciting structures (JH, 1/2SVFSE), although the diffusion component does contribute to a performance improvement compared to the pure jump case, its added value does not seem to justify the increase in complexity of the parameter space: the IVRMSEs generated by the 1SVFSE and 2SVFSE models are respectively 80% and 79% below the benchmark, compared to 74% reduction offered by the JH model. Similar considerations can be drawn from the analysis of other performance measures such as the average absolute error in prices (APEs) - in particular we observe that the APEs of each model are below the 5% threshold

		1 SV Factor Models					2 SV Factor Models					
		Heston	JH	JBNS	SVFSE	SVFHO	Heston	SVFSE	SVFHO			
$v(t)$	$v(0)$	0.0080	0.0601	0.4020	0.0592	0.2932	0.0040	0.0086	0.0090	0.0490	0.0320	0.6122
	$\kappa$	6.2669	0.1452	2.2777	14.9999	1.6780	1.2034	1.1828	0.0226	0.1056	1.0903	38.9138
	$\theta$	0.0304	1.9732	0.0009	0.0163	0.4783	0.0229	0.0357	1.2741	2.1060	5.6149	0.1662
	$\eta_{1,D}$	1.4782	-	-	0.2355	1.3548	0.2339	1.5000	0.7146		1.5000	
	$\rho$	-0.7217	-	-	-0.9930	-0.6988	-0.8287	-0.8376	-1.0000		-0.8701	
	$\eta_{1,J}$	-	0.5523	1.0000	0.7578	0.8163	-	-	0.5038		0.3451	
$X(t)$	$\sigma_{1,D}$	1.0000	-	-	0.2807	0.1511	1.0000	1.0000	0.5015		0.1860	
	$\sigma_{1,J}$	-	0.2358	0.2966	0.3336	0.2459	-	-	0.3311		0.4389	
CGMY	C	-	1.0700	0.4809	2.9065	0.9719	-	-	0.8534		0.2810	
	G	-	0.3788	1.3619	1.8144	1.6223	-	-	0.5994		2.0984	
	M	-	6.8541	8.7153	9.9163	6.7453	-	-	8.6046		13.8537	
	Y	-	1.5641	0.8390	0.8614	0.1450	-	-	1.4579		0.9843	
IVRMSE		0.0090	0.0023	0.0068	0.0018	0.0020	0.0056		0.0019		0.0031	
$\Delta$ IVRMSE		-	-74.34%	-23.66%	-80.32%	-77.86%	-37.72%		-79.01%		-64.96%	
APE Price (%)		1.90%	0.30%	1.70%	0.28%	0.40%	0.34%		0.23%		0.58%	
N. Parameters		6	9	9	12	12	12		15		15	

Table 3: Parameter Estimates and Option Fit: Calibration Exercise 1. Data: S&P500 options observed at 24/04/2017. Source Bloomberg. Base process: CGMY. IVRMSE: implied volatility root mean square error.  $\Delta$ IVRMSE =  $(\text{IVRMSE}_{mod} - \text{IVRMSE}_{Heston}) / \text{IVRMSE}_{Heston}$ : reduction in the IVRMSE offered by given model compared to Heston model. APE Price =  $(\sum_{options} |\text{price}_{mod} - \text{price}_{mkt}|) / \text{mean option price}$ : average absolute error in price as percentage of the mean option price.

		1 SV Factor Models					2 SV Factor Models		
Date		Heston	JH	JBNS	SVFSE	SVFHOU	Heston	SVFSE	SVFHOU
20/03/2020	IVRMSE	0.0217	0.0164	0.0165	0.0163	0.0162	0.0214	0.0156	0.0156
	$\Delta$ IVRMSE	-	-24.45%	-24.34%	-25.26%	-25.43%	-1.57%	-28.08%	-28.50%
	APE Price (%)	2.15%	1.96%	1.98%	2.02%	2.00%	2.00%	1.91%	1.92%
24/04/2020	IVRMSE	0.0187	0.0034	0.0120	0.0033	0.0037	0.0152	0.0039	0.0030
	$\Delta$ IVRMSE	-	-81.78%	-35.91%	-82.22%	-80.47%	-18.93%	-79.03%	-84.20%
	APE Price (%)	2.30%	0.39%	1.43%	0.39%	0.41%	1.91%	0.38%	0.34%
11/05/2021	IVRMSE	0.0087	0.0040	0.0078	0.0051	0.0039	0.0087	0.0027	0.0068
	$\Delta$ IVRMSE	-	-54.32%	-10.89%	-41.38%	-55.19%	-1.00%	-69.18%	-21.74%
	APE Price (%)	1.26%	0.69%	1.01%	0.77%	0.54%	1.26%	0.36%	1.06%
	N. Parameters	6	9	9	12	12	12	15	15

Table 4: Option Fit: Calibration Exercise 1. Data S&P500 options. Source Bloomberg. Base Process CGMY. IVRMSE: implied volatility root mean square error.  $\Delta$ IVRMSE =  $(\text{IVRMSE}_{mod} - \text{IVRMSE}_{Heston})/\text{IVRMSE}_{Heston}$ : reduction in the IVRMSE offered by given model compared to Heston model. APE Price =  $(\sum_{options} |\text{price}_{mod} - \text{price}_{mkt}|)/\text{mean option price}$ : average absolute error in price as percentage of the mean option price.

indicated by Carr et al. (2007). In this respect, the JH model proves to be very competitive mainly due to its limited number of parameters which makes it a more parsimonious alternative compared to other specifications.

The above reported analysis refers to a date characterised by a low level of the CBOE VIX index: on 24/04/2017 in fact the VIX closed at 10.8. We further investigate the models calibration performance for three other representative days in recent years with medium, high and exceptionally high levels of the VIX. In details we consider S&P500 options quotes on 20/03/2020 with VIX at 66 (exceptionally high level), 24/04/2020 with VIX at 35.9 (high level), and 11/05/2021 with VIX at 21.8 (medium level). Quotes are extracted from Bloomberg, and the dataset for each date has the same specifics as the one used above. In the interest of space, in Table 4 we report only the IVRMSEs and APEs generated by the calibration of each model (fuller details concerning the calibrated parameters are available upon request). The results confirm the conclusions from the previous analysis. We note in particular the performance measures for March 2020, when the financial markets were particularly unstable following the announcement that the COVID-19 outbreak had been declared a pandemic by the World Health Organization (WHO, 2020). Even in such conditions the families of models studied in this paper manage to provide a good calibration performance with respect to the measures considered so far.

Further insights into the performance of each model could be gained by studying their ability of generating a plausible (meant as consistent with intuition as well as the no arbitrage principle) forward implied volatility smile. We extract this surface from the prices at inception (time  $t = 0$ ) of forward start options with payoff  $(S(T)/S(t) - k)^+$ , where  $T$  is the contract maturity, and  $t \in (0, T)$  denotes the determination date of the strike. This is defined via the strike ratio  $k = K/S(t)$ , so that the effective strike price  $K$  is a multiple of the underlying asset price at  $t$ . Thus, the strike is determined at a later date  $t$  with respect to inception, however at  $t$  the contract turns into a vanilla European option. Prices are computed using the COS method (Fang and Oosterlee, 2008) with the forward characteristic function obtained in Proposition 3.

In order to investigate in details the features of the forward smile induced by the models,

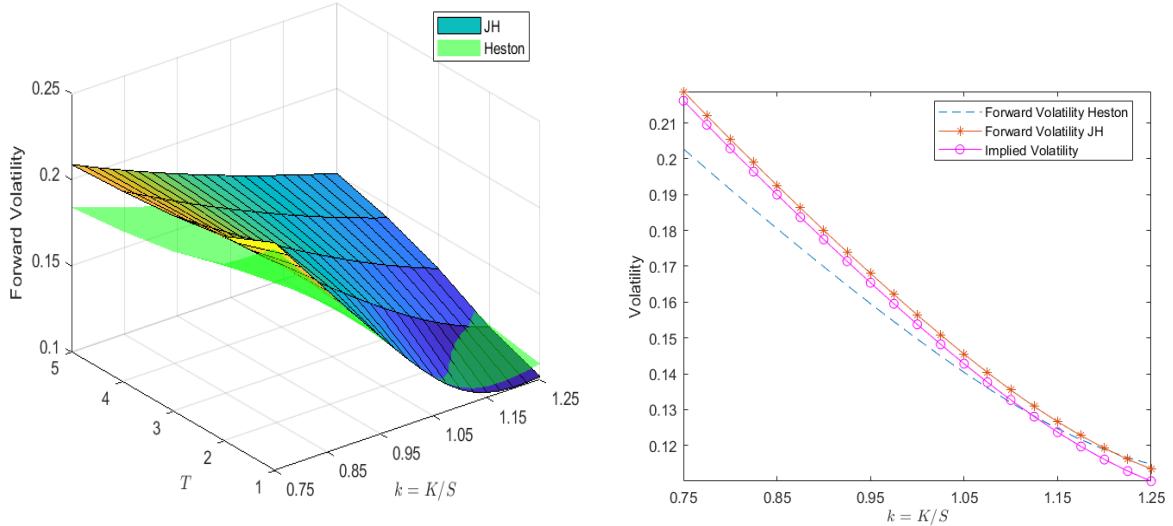


Figure 3: Forward Volatility: JH vs Heston - determination date  $t = 1$  month. Left hand side panel: time to maturity  $T - t$  ranging from 11 to 59 months, i.e. contracts with maturity ranging from 1 to 5 years from inception. Right hand side panel:  $T = 2$  years, time to maturity  $T - t = 23$  months. Forward start options priced using the COS method and the forward characteristic function in Proposition 3. Parameter set: Table 3

we consider the following two cases. The first one is the case of a forward start option with determination date in 1 month. Given the close determination date, and the relatively long time to maturity ( $T - 1$  month), we would expect the forward volatility to be higher but relatively close to the implied volatility extracted from vanilla options with the same time to maturity. The second case instead is the one a forward start option with fixed time to maturity of 1 month, so that the actual determination date is  $t = T - 1$  month, i.e. quite further ahead in time compared to the previous situation. This would mean higher uncertainty concerning both the price and its volatility level. Consequently, we would expect significantly higher level of forward volatility compared to the implied volatility obtained from corresponding vanilla options.

These two cases are illustrated in Figures 3 and 4 respectively, in which we focus our attention primarily on the JH model and the benchmark Heston model. Both figures show patterns of the JH forward volatility which are consistent with the intuition reported above. In comparison the forward volatility surface under the Heston model is flatter and characterised by unrealistically lower values: the right hand side panel of Figure 3 in particular shows it is counter-intuitively lower than the corresponding implied volatility. The forward volatility surface of the JH model is relatively convex for contracts with short time to maturity (left hand side panels of Figure 4); however, the convexity effect is particularly accentuated in the 2SVFSE model (right hand side panels of Figure 4). All the other models considered in this paper show very similar shapes for the forward volatility, with the only exception of the JBNS model, which produces much lower levels compared to the benchmark (full results available upon request).

More meaningful indications could be extracted from the joint calibration of the models to market quotes for both vanilla and forward start options. However this is not possible at this stage due to lack of publicly available quotes for these exotic instruments. Nevertheless, this experiment shows that the increased distribution flexibility offered by some of the models included in our setup

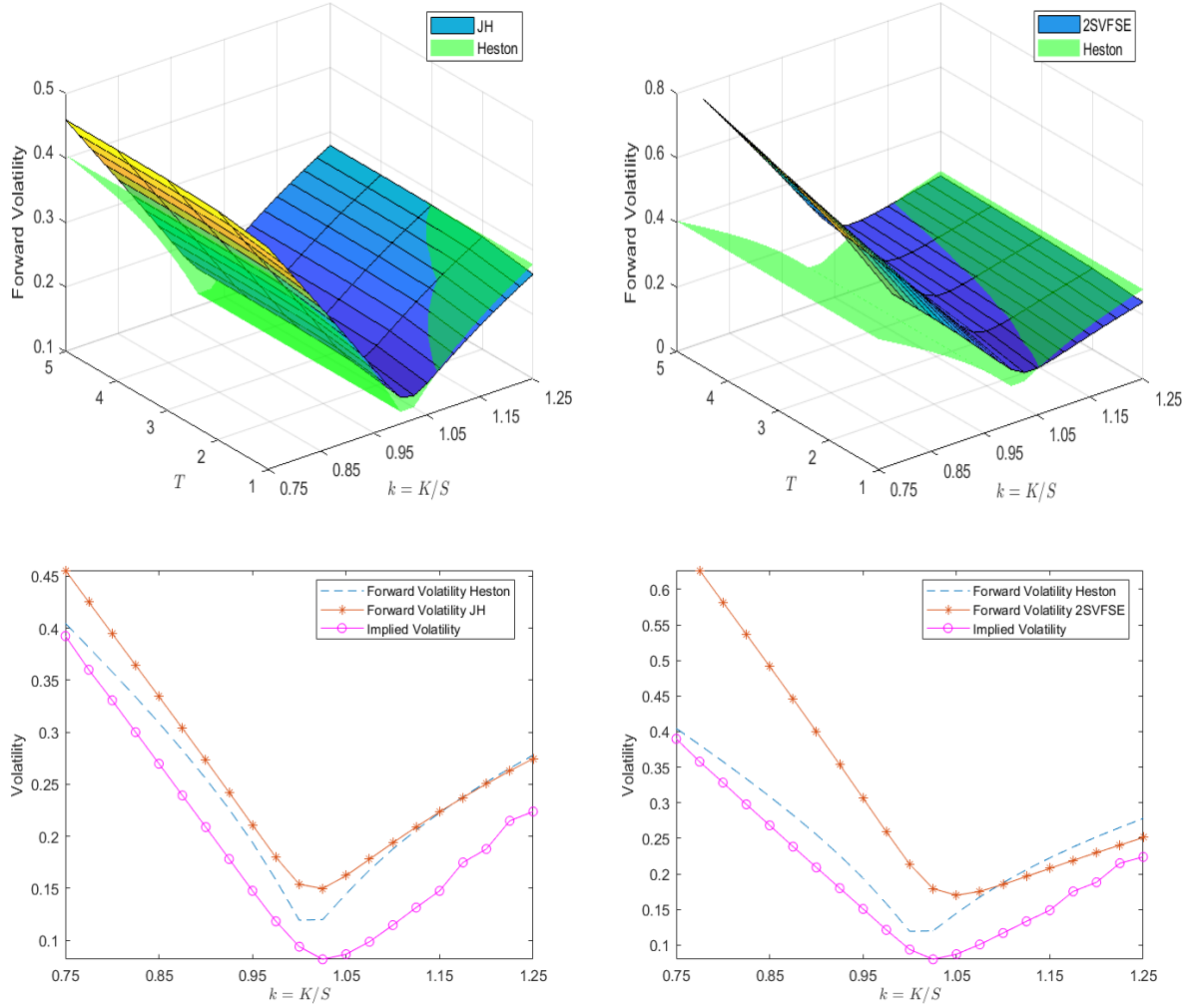


Figure 4: Forward Volatility: JH/2SVFSE vs Heston - time to maturity  $T - t = 1$  month. Top panels: determination date  $t$  ranging from 11 to 59 months, i.e. contracts with maturity ranging from 1 to 5 years from inception. Bottom panels:  $T = 2$  years, determination date  $t = 23$  months. Forward start options priced using the COS method and the forward characteristic function in Proposition 3. Parameter set: Table 3.

enhances their ability to generate richer and plausible patterns for the forward volatility. In this context, we further mention Rebonato (2020), who uses future conditional densities obtained by superposition of log-normal distributions.

We conclude by observing that the calibrated value of the parameter  $Y$  is always positive, indicating infinite activity jumps. Thus, in unreported experiments, we repeat this calibration exercise by adding the constraint  $Y < 0$ , in order to study the resulting fit of a specification corresponding to a compound Poisson jump structure with jump size following an asymmetric double gamma distribution (Ballotta and Kyriakou, 2014), similar in spirit to the constructions of Duffie et al. (2000) and Andersen et al. (2015) for example. The results indicate an overall deterioration of the fit quality across all models considered so far, confirming the inadequacy of the traditional low frequency compound Poisson specification (see also Huang and Wu, 2004, for example).

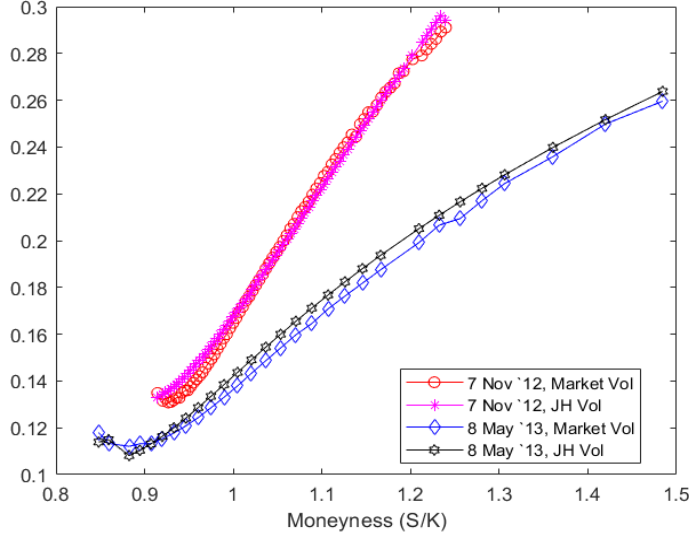


Figure 5: Volatility smirks: JH model for selected dates and maturities. Implied volatilities for options on two different days: November 11, 2012, 45 days to maturity contracts; May 8, 2013, 227 days to maturity options. Market Vol: market implied volatility. JH Vol: implied volatility from the calibrated JH model. Data: S&P500 options. Observation period: 4/09/2012 - 29/08/2014. IVRMSE: 0.0049, 0.0052 respectively.

**Calibration Exercise 2.** We refer to Wednesday quotes for options on the S&P500 from September 2012 to the end of August 2014; the dataset is then divided in two sub-dataset - from September 4th 2012 to August 28th 2013 (20,525 contracts) and from September 4th 2013 to August 27th 2014 (18,066 contracts). Moneyness and maturities span respectively from 0.83 to 1.49 and 5 to 1031 business days (full details in Appendix B).

We use the first sub-dataset to calibrate all the models and select the parameters (‘in-sample’) by solving the optimization problems (27)–(28) for  $T = 52$  observation dates. Then, we update only  $v(t)$  at each observation date in the second sub-dataset by solving the optimization problem (28) for  $T = 50$  observation dates with the set of model parameters  $\Theta^*$  fixed (‘out-of-sample’).

Results are summarized in Table 5.A (fuller analysis provided in Appendix C), and confirm the findings of the Calibration Exercise 1, specifically the superior performance of the self-exciting structures. The JH model, in particular, proves its competitiveness thanks to its relatively small number of parameters and its robustness, for which it can offer a reduction of up to 54% in the calibration error with respect to the benchmark. For illustration, in Figure 5 we report the market implied volatilities on two different dates of the dataset together with the corresponding implied volatilities generated by JH model. The figure includes a set of short dated options with relatively high volatility and a set of long dated contracts with relatively low volatility. We note the jumps have infinite variation (the optimal values of  $Y$  is 1.71).

Finally, in order to assess the models performances irrespective of the benchmark, and en route identify possible discriminant model features, we carry out a pairwise Equal Predictive Accuracy (EPA) test based on the following  $t$ -statistics, which uses as relevant loss function the (weekly) implied volatility mean squared errors (IVMSE)

$$t\text{-statistics} = \frac{\text{sample average}(\text{IVMSE}_i - \text{IVMSE}_j)}{\text{st. dev.}(\text{IVMSE}_i - \text{IVMSE}_j)}, \quad (29)$$

(see Diebold and Mariano, 1995, and for a similar study Huang and Wu, 2004, as well). We apply the Newey-West correction for heteroskedasticity and autocorrelation. A positive  $t$ -value implies that the IVMSE from model  $i$  is significantly larger than the IVMSE from model  $j$ ; in other words, model  $j$  outperforms model  $i$ . A negative  $t$ -value implies the opposite. Results are reported in Panels B–D of Table 5, which also show the corresponding  $p$ -values.

In details, we first investigate the best possible construction in terms of nature of the risk drivers to be included in the relevant dynamics. Thus, in Table 5.B, we test the null hypothesis of equal predictive ability of ‘pure diffusion’ models (i.e. Heston and its 2 SV factor version) in comparison to models based on either purely discontinuous dynamics (JH and JBNS), or both diffusive and discontinuous components (1/2SVFSE and 1/2SVFHOU). From these results, the null hypothesis is rejected, as ‘diffusion-only’ models are not sufficient to reproduce accurately the observed market volatility surfaces. Indeed, the Heston model and its 2 stochastic volatility factor version return errors which are consistently larger than the ones generated by other models.

Secondly, in Table 5.C we compare the performance of the purely discontinuous models (JBNS and JH) with their counterparts combining also diffusion (1/2SVFSE and 1/2SVFHOU). The results confirm the relative competitiveness of the JH model, thus showing that jumps alone can produce satisfactory model fit.

In Table 5.D, we test the predictive accuracy of both jump structures considered in this paper, i.e. the finite variation non-Gaussian OU versus the infinite variation self-exciting class. Results highlight the superior performance of the 2SVFHOU model when compared to models based on the self exciting structure, with the only exception of the JH model (we note the ‘borderline’  $p$ -value at 10% significance level).

We conclude this section with the following remark. The analysis of the ‘out-of-sample’ performance metrics could be extended to longer datasets as to further investigate the stability of the calibrated parameters in greater details. On the other hand, as markets are in general non stable, in the financial industry model parameters are recalibrated with frequency depending on the prevailing conditions. Furthermore, on occasions additional provisions based on sophisticated risk measures such as Value at Risk, for example, might be included in order to address regulatory constraints, and instances of irrational market behaviour. Potential resulting fluctuations in the relevant risk measure could be monitored via ‘devolatilization’ as discussed in Eberlein et al. (2003) and references therein.

## 5 Conclusions

We propose a general framework for the joint evolution of stock log-returns and their volatility using TCLP with stochastic volatility and leverage effects originating from both diffusion and purely discontinuous processes. The setup admits analytical results for the characteristic function and the forward characteristic function of the log-returns, which facilitate the efficient pricing of vanilla and forward-start options. The framework shows robust performance in terms of calibration to market quotes, as well as richer and plausible forward volatility smile patterns. The analysis also identifies a versatile new pure jump construction, which we christened JH model.

The analysis of the forward volatility smile that can be extracted from the models proposed in this paper indicates their potential also at controlling for model risk - a crucial issue faced by

PANEL A: Calibration performance - model IVRMSE

	Heston	JH	JBNS	1SVFSE	1SVFHOU	Heston 2F	2SVFSE	2SVFHOU
'In-Sample'	0.0099	0.0073	0.0233	0.0090	0.0121	0.0073	0.0070	0.0067
'Out-of-Sample'	0.0187	0.0087	0.0165	0.0123	0.0107	0.0123	0.0071	0.0102

PANEL B: Pairwise EPA. Which risk factors perform best - Pure Diffusion vs 'Non Diffusion'  
'In-Sample'

Heston	JBNS	1SVFHOU	2SVFHOU	JH	1SVFSE	2SVFSE
1 SV Factor	-5.1642 (2.02E-06)	-1.7012 (0.0475)	5.2719 (1.38E-06)	5.4334 (7.80E-07)	1.4519 (0.0763)	5.1466 (2.14E-06)
2 SV Factor	-6.4290 (2.17E-08)	-2.9293 (0.0025)	2.6213 (0.0058)	0.4085 (0.3423)	-3.3742 (0.0007)	1.3796 (0.0869)

Heston	JBNS	1SVFHOU	2SVFHOU	JH	1SVFSE	2SVFSE
1 SV Factor	1.2333 (0.1117)	5.8633 (1.90E-07)	7.4452 (6.80E-10)	7.5652 (4.44E-10)	4.7809 (8.16E-06)	7.6701 (3.06E-10)
2 SV Factor	-4.7645 (8.63E-06)	2.2498 (0.0145)	3.5324 (0.0005)	5.5672 (5.39E-07)	0.1402 (0.4445)	6.1960 (5.83E-08)

PANEL C: Pairwise EPA. Which risk factors perform best - Pure Jump vs 'Jump Diffusion'  
'In-Sample'

	1 SVFHOU	2SVFHOU	1 SVFSE	2SVFSE
JBNS	4.7774 (7.71E-06)	6.5050 (1.65E-08)	5.8089 (2.04E-07)	6.5719 (1.29E-08)
JH	-2.8144 (0.0035)	2.3949 (0.0102)	-2.8055 (0.0035)	2.3359 (0.0117)

	1 SVFHOU	2SVFHOU	1 SVFSE	2SVFSE
JBNS	5.4312 (8.68E-07)	5.2457 (1.66E-06)	3.5895 (3.82E-04)	6.8930 (4.86E-09)
JH	-2.5717 (0.0066)	-2.9659 (0.0023)	-4.6142 (1.43E-05)	6.8852 (4.99E-09)

PANEL D: Pairwise EPA. Which jump structure performs best - OU vs Self Exciting  
'In-Sample'

	JH	1SVFSE	2SVFSE	JH	1SVFSE	2SVFSE
JBNS	6.4009 (2.40E-08)	5.8089 (2.04E-07)	6.5719 (1.29E-08)	6.3373 (3.53E-08)	3.5895 (3.82E-04)	6.8930 (4.86E-09)
1SVFHOU	2.8144 (0.0035)	2.4080 (0.0098)	2.9379 (0.0025)	2.5717 (0.0066)	-1.9845 (0.0264)	4.2585 (4.64E-05)
2SVFHOU	-2.3949 (0.0102)	-3.6169 (0.0003)	-0.9801 (0.1658)	2.9659 (0.0023)	-2.5425 (0.0071)	5.3776 (1.05E-06)

Table 5: Model IVRMSE from calibration to market data and pairwise EPA  $t$ -statistics. Data S&P500 options. Observation period: 4/09/2012 - 29/08/2014. Source: OptionMetrics. Base process: CGMY. EPA  $t$ -statistics defined in equation (29); corresponding  $p$ -values reported in parenthesis. Panel A - IVRMSE. Panel B - Model<sub>i</sub>: Heston (classic and 2 SV factor); Model<sub>j</sub>: JBNS, 1/2SVFHOU, JH, 1/2SVFSE. Panel C - Model<sub>i</sub>: pure jump (JBNS, JH); Model<sub>j</sub>: 1/2SVFHOU, 1/2SVFSE. Panel D - Model<sub>i</sub>: non-Gaussian OU based models (JBNS, 1/2SVFHOU); Model<sub>j</sub>: self-exciting structure based models (JH, 1/2SVFSE).

financial institutions for their risk management strategies. In this respect, it would be interesting to further assess the performance of the models along the lines of Coqueret and Tavin (2016). Indeed, given their results on the amount of model risk carried by pure jump models, which could be broadly casted into the OU setting of our general framework, it would be appropriate to also investigate the performance of our self exciting structures with endogenous stochastic volatility of volatility and leverage; we leave this topic to further research.

Additional directions for further research could be articulated as follows. In primis, the study of more efficient numerical schemes for models with no explicit expressions for the characteristic function, like the ones explored in this paper is of interest. Artificial neural networks in the spirit of Liu et al. (2019a,b) for example could prove particularly helpful in this respect, and are currently being investigated. Given the attention of practitioners on the hedging of exotic products (which in the equity market account for about 55% of the notional amount outstanding), another possible avenue of research would be the investigation of the performance of the JH model for the pricing of these products by suitably extending the numerical schemes proposed by Cui et al. (2017, 2019) to cater for jump-induced leverage. Further research could also be carried out to develop expansions of the shape characteristics of the implied volatility surface generated by the models proposed in this paper on the line of Aït-Sahalia et al. (2020, 2021). An equally interesting topic would be the extension of the model-free approach to calibration of Cui et al. (2021) to allow for time changes as advocated in this paper.

Other relevant directions would be the analysis of the performance of the general framework proposed in this paper against VIX derivatives and other variance products in the spirit of Fouque and Saporito (2018) and Kaeck and Seeger (2020), and in terms of joint calibration of the smile of S&P options and VIX options (see Guyon, 2020, for further details).

## Acknowledgements

The Authors would like to thank Lorenzo Bergomi, Peter Carr, Ernst Eberlein, Vladimir Lucic, Dilip Madan, Marek Musiela and Gregory Pelts for useful comments and suggestions. A previous version of this manuscript has been circulated with the title ‘Smiles & Smirks: a tale of factors’. This paper has been presented at the 9th and 10th World Congress of the Bachelier Finance Society, QuantMinds International 2018, the Quant Insights Conference 2017, the 2nd International Conference on Computational Finance ICCF 2017, the 2017 Global Derivatives Conference, the 2017 Actuarial and Financial Mathematics Conference in Brussels, and seminars at Università degli Studi di Milano - Bicocca, and University of Sussex. We thank all the participants for their helpful feedback. All remaining errors are exclusively ours, and the views expressed in this paper do not necessarily represent those of Belfius Bank. Usual caveat applies.

## References

- Aït-Sahalia, Y., 2004. Disentangling diffusion from jumps. *Journal of Financial Economics* 74, 487 – 528.
- Aït-Sahalia, Y., Li, C., Li, C.X., 2020. Implied stochastic volatility models. *The Review of Financial Studies* 34, 394–450.

- Aït-Sahalia, Y., Li, C., Li, C.X., 2021. Closed-form implied volatility surfaces for stochastic volatility models with jumps. *Journal of Econometrics* 222, 364–392.
- Andersen, T.G., Fusari, N., Todorov, V., 2015. The risk premia embedded in index options. *Journal of Financial Economics* 117, 558 – 584.
- Backus, D.K., Foresi, S., Wu, L., 2004. Accounting for biases in Black-Scholes. *SSRN Electronic Journal* .
- Ballotta, L., Bonfiglioli, E., 2014. Multivariate asset models using Lévy processes and applications. *The European Journal of Finance* 22, 1320–1350.
- Ballotta, L., Deelstra, G., Rayée, G., 2017. Multivariate FX models with jumps: triangles, quantos and implied correlation. *European Journal of Operational Research* 260, 1181–1199.
- Ballotta, L., Fusai, G., Marazzina, D., 2019. Integrated structural approach to Credit Value Adjustment. *European Journal of Operational Research* 272, 1143–1157.
- Ballotta, L., Kyriakou, I., 2014. Monte Carlo simulation of the CGMY process and option pricing. *Journal of Futures Markets* 34, 1095–1121.
- Barndorff-Nielsen, O.E., Shephard, N., 2003. Integrated OU processes and non-Gaussian OU-based stochastic volatility models. *Scandinavian Journal of Statistics* 30, 277–295.
- Bates, D.S., 1996. Jumps and stochastic volatility: Exchange rate processes implicit in Deutsche Mark options. *The Review of Financial Studies* 9, 69–107.
- Bergomi, L., 2015. *Stochastic Volatility Modeling*. Chapman and Hall/CRC.
- BIS, 2019. Statistical release: OTC derivatives statistics at end December 2018.
- Black, F., Scholes, M., 1973. The pricing of options and corporate liabilities. *Journal of Political Economy* 81, 637–654.
- Callegaro, G., Fiorin, L., Grasselli, M., 2019. Quantization meets Fourier: a new technology for pricing options. *Annals of Operations Research* 282, 59–86.
- Carr, P., Geman, H., Madan, D.B., Yor, M., 2002. The fine structure of asset returns: An empirical investigation. *Journal of Business* 75, 305–332.
- Carr, P., Geman, H., Madan, D.B., Yor, M., 2003. Stochastic volatility for Lévy processes. *Mathematical Finance* 13, 345–382.
- Carr, P., Geman, H., Madan, D.B., Yor, M., 2007. Self-decomposability and option pricing. *Mathematical Finance* 17, 31–57.
- Carr, P., Wu, L., 2004. Time-changed Lévy processes and option pricing. *Journal of Financial Economics* 71, 113–141.
- Carr, P., Wu, L., 2007. Stochastic skew in currency options. *Journal of Financial Economics* 86, 213–247.
- Carr, P., Wu, L., 2017. Leverage effect, volatility feedback, and self-exciting market disruptions. *Journal of Financial and Quantitative Analysis* 52, 2119–2156.
- Cheng, P., Scaillet, O., 2007. Linear-quadratic jump-diffusion modeling. *Mathematical Finance* 17, 575–598.
- Christoffersen, P., Heston, S., Jacobs, K., 2009. The shape and term structure of the index option smirk: Why multifactor stochastic volatility models work so well. *Management Science* 55, 1914–1932.

- Coqueret, G., Tavin, B., 2016. An investigation of model risk in a market with jumps and stochastic volatility. *European Journal of Operational Research* 253, 648–658.
- Cui, Z., Kirkby, J.L., Nguyen, D., 2017. A general framework for discretely sampled realized variance derivatives in stochastic volatility models with jumps. *European Journal of Operational Research* 262, 381–400.
- Cui, Z., Kirkby, J.L., Nguyen, D., 2019. A general framework for time-changed Markov processes and applications. *European Journal of Operational Research* 273, 785–800.
- Cui, Z., Kirkby, J.L., Nguyen, D., 2021. A data-driven framework for consistent financial valuation and risk measurement. *European Journal of Operational Research* 289, 381–398.
- Diebold, F.X., Mariano, R.S., 1995. Comparing predictive accuracy. *Journal of Business & Economic Statistics* 13, 253–263.
- Duffie, D., Pan, J., Singleton, K., 2000. Transform analysis and asset pricing for affine jump-diffusions. *Econometrica* 68, 1343–1376.
- Eberlein, E., 2013. Fourier based valuation methods in mathematical finance, in: Benth, F.e., Kholodnyi, V.A., Laurence, P. (Eds.), *Quantitative Energy Finance. Modeling, Pricing, and Hedging in Energy and Commodity Markets*. Springer, pp. 85–114.
- Eberlein, E., Glau, K., Papapantoleon, A., 2010. Analysis of Fourier transform valuation formulas and applications. *Applied Mathematical Finance* 17, 211–240.
- Eberlein, E., Kallsen, J., 2019. *Mathematical Finance*. Springer.
- Eberlein, E., Kallsen, J., Kristen, J., 2003. Risk management based on stochastic volatility. *The Journal of Risk* 5, 19–44.
- Eberlein, E., Keller, U., 1995. Hyperbolic distributions in finance. *Bernoulli* 1, 281–299.
- Eraker, B., 2004. Do stock prices and volatility jump? Reconciling evidence from spot and option prices. *Journal of Finance* 59, 1367–1403.
- Eraker, B., Johannes, M., Polson, N., 2003. The impact of jumps in volatility and returns. *Journal of Finance* 58, 1269–1300.
- Fallahgoul, H., Loeper, G., 2019. Modelling tail risk with tempered stable distributions: an overview. *Annals of Operations Research* .
- Fang, F., Oosterlee, C.W., 2008. A novel pricing method for European options based on Fourier-Cosine series expansions. *SIAM Journal on Scientific Computing* 31, 826–848.
- Fouque, J.P., Saporito, Y.F., 2018. Heston stochastic vol-of-vol model for joint calibration of VIX and S&P 500 options. *Quantitative Finance* 18, 1003–1016.
- Fulop, A., Li, J., Yu, J., 2014. Self-exciting jumps, learning, and asset pricing implications. *Review of Financial Studies* 28, 876–912.
- Gatheral, J., 2006. *The Volatility Surface: A Practitioner’s Guide*. WILEY.
- Gatheral, J., Jacquier, A., 2014. Arbitrage-free SVI volatility surfaces. *Quantitative Finance* 14, 59–71.
- Guyon, J., 2020. The joint S&P 500/VIX smile calibration puzzle solved. *Risk* April, 1–6.

- Heston, S., 1993. A closed-form solution for options with stochastic volatility with applications to bond and currency options. *The Review of Financial Studies* 6, 327–343.
- Huang, J.Z., Wu, L., 2004. Specification analysis of option pricing models based on time-changed Lévy processes. *Journal of Finance* 59, 1405–1439.
- Jacod, J., 1979. Calcul stochastique et problèmes de martingales. volume 714 of *Lecture Notes in Mathematics*. Springer.
- Kaeck, A., Seeger, N.J., 2020. VIX derivatives, hedging and vol-of-vol risk. *European Journal of Operational Research* 283, 767–782.
- Kallsen, J., 2006. A didactic note on affine stochastic volatility models, in: Kabanov, Y., Liptser, R., Stoyanov, J. (Eds.), *From Stochastic Calculus to Mathematical Finance*. The Shiryaev Festschrift. Springer, pp. 343–368.
- Kallsen, J., Muhle-Karbe, J., Voß, M., 2011. Pricing options on variance in affine stochastic volatility models. *Mathematical Finance* 21, 627–641.
- Kirkby, J.L., 2015. Efficient option pricing by frame duality with the fast Fourier transform. *SIAM Journal on Financial Mathematics* 6, 713–747.
- Küchler, U., Sørensen, M., 1997. *Exponential Families of Stochastic Processes*. Springer Series in Statistics, Springer.
- Li, C., Wu, L., 2019. Exact simulation of the Ornstein-Uhlenbeck driven stochastic volatility model. *European Journal of Operational Research* 275, 768 – 779.
- Liu, S., Borovykh, A., Grzelak, L.A., Oosterlee, C.W., 2019a. A neural network-based framework for financial model calibration. *Journal of Mathematics in Industry* 9.
- Liu, S., Oosterlee, C., Bohte, S., 2019b. Pricing options and computing implied volatilities using neural networks. *Risks* 7, 16.
- Madan, D.B., Carr, P., Chang, E., 1998. The Variance Gamma process and option pricing. *European Finance Review* 2, 79–105.
- Merton, R.C., 1976. Option pricing when underlying stock returns are discontinuous. *Journal of Financial Economics* 3, 125–144.
- Ornathanalai, C., 2014. Lévy jump risk: Evidence from options and returns. *Journal of Financial Economics* 112, 69 – 90.
- Pan, J., 2002. The jump-risk premia implicit in options: evidence from an integrated time-series study. *Journal of Financial Economics* 63, 3–50.
- Pun, C.S., Chung, S.F., Wong, H.Y., 2015. Variance swap with mean reversion, multifactor stochastic volatility and jumps. *European Journal of Operational Research* 245, 571 – 580.
- Rebonato, R., 2020. What does today’s smile imply about future volatilities? *The Journal of Derivatives* 27, 26–44.
- Revuz, D., Yor, M., 1991. Continuous Martingales and Brownian motion. volume 293 of *A Series of Comprehensive Studies in Mathematics*. Springer-Verlag, Berlin.
- Santa-Clara, P., Yan, S., 2010. Crashes, volatility, and the equity premium: Lessons from S&P 500 options. *The Review of Economics and Statistics* 92, 435–451.

Schoutens, W., Simons, E., Tistaert, J., 2005. Model risk for exotic and moment derivatives, in: Kyprianou, A., Schoutens, W., Wilmott, P. (Eds.), *Exotic Option Pricing and Advanced Lévy Models*. chapter 4, pp. 67–97.

Sepp, A., 2008. Pricing options on realized variance in the Heston model with jumps in returns and volatility. *The Journal of Computational Finance* 11, 33–70.

WFE, 2019. 2018 Derivatives Market Survey.

WHO, 2020. WHO director-general’s opening remarks at the media briefing on COVID-19 - 11 March 2020.

## Appendix

### A Time changed Lévy processes: the affine case. Setup and proofs of Propositions

In the set up used to define the market model in Section 3,  $(v, X)$  is modelled as a  $\mathbb{R}^+ \times \mathbb{R}$ -valued bivariate affine process with differential characteristic  $(B, \Sigma, K)$ , relative to the canonical truncation function, of the form

$$\begin{aligned} B &= \begin{pmatrix} \kappa\theta - \eta_{0,J}\tilde{\alpha}_0 \\ -\varphi_0(-i) + \sigma_{0,J}\alpha_0 \end{pmatrix} + \begin{pmatrix} -\kappa - \eta_{1,J}\tilde{\alpha}_1 \\ -\varphi_1(-i) + \sigma_{1,J}\alpha_1 \end{pmatrix} v \\ \Sigma &= \begin{pmatrix} \eta_{1,D}^2 & \eta_{1,D}\sigma_{1,D}\rho \\ \eta_{1,D}\sigma_{1,D}\rho & \sigma_{1,D}^2 \end{pmatrix} v \\ K(G) &= K_0(G) + K_1(G)v, \quad \forall G \in \mathcal{B}(\mathbb{R}^2), \end{aligned}$$

with  $K(\cdot)$  denoting the measure of the compensator term in the differential characteristic of the bivariate affine process  $(v(t), X(t))$ , and  $K_0(\cdot)$ ,  $K_1(\cdot)$  the Lévy measures of the bivariate jumps process in  $v$  and  $X$ . These are functions of  $\nu_j$  and  $\tilde{\nu}_j$ ,  $j = 0, 1$ , the specification of which depends on the parameter setting. For example, in the JH (and the 1SVFSE) model  $K_0(\cdot) = 0$  and

$$K(G) = \left( \int 1_G(-\eta_{1,J}z, \sigma_{1,J}y)\nu_{1,-}(dz) + \int 1_G(0, \sigma_{1,J}y)\nu_{1,+}(dy) \right) v(t), \quad G \in \mathcal{B}(\mathbb{R}^2),$$

whilst in the JBNS (and the 1SVFHOU) model

$$\begin{aligned} K(G) &= \int 1_G(-\eta_{0,J}z, 0)\nu_{1,-}(dz) \\ &+ \left( \int 1_G(0, \sigma_{1,J}z)\nu_{1,-}(dz) + \int 1_G(0, \sigma_{1,J}y)\nu_{1,+}(dy) \right) v(t), \quad G \in \mathcal{B}(\mathbb{R}^2). \end{aligned}$$

We observe that the quadratic variation process of the TCLP  $X(t) = L(T(t))$  introduced in Section 2.1 is

$$[X](t) = \sigma^2 T(t) + \int_0^t \int_{\mathbb{R}} x^2 \mu(dx, ds),$$

where  $\mu(dx, dt)$  is the integer valued random measure of the jumps of  $X$  with compensator  $\nu(dx)v(t)dt$ . Therefore

$$\langle X \rangle(t) = \sigma^2 T(t) + \int_0^t \int_{\mathbb{R}} x^2 \nu(dx)v(s)ds = \text{Var}(L(1))T(t)$$

(see Eberlein and Kallsen, 2019, Carr et al., 2003, as well). Consequently, equation (14) follows from the above, in conjunction with equation (3) and bearing in mind that  $L_0$  and  $L_1$  are independent.

Concerning equations (15) and (16), we illustrate the relevant argument using the 1SVFSE model as an example, and recognizing that similar arguments hold for all other models analysed

in this paper. Note, that for readability we use the differential notation. Thus

$$d\langle v \rangle(t) = (\eta_{1,D}^2 + \eta_{1,J}^2 \mathbb{V}ar(J_{1,-}(1))) v(t) dt,$$

and consequently by equation (4)

$$q(t) = \gamma_1^2 (\eta_{1,D}^2 + \eta_{1,J}^2 \mathbb{V}ar(J_{1,-}(1))) v(t).$$

In this case the contribution from the jump part is  $q_J(t) = \eta_{1,J}^2 \mathbb{V}ar(J_{1,-}(1)) v(t)$ . Similarly, as  $J_{1,-}$  and  $J_{1,+}$  are independent, then

$$d\langle X, v \rangle(t) = (\sigma_{1,D} \eta_{1,D} \rho dt - \sigma_{1,J} \eta_{1,J} \mathbb{V}ar(J_{1,-}(1))) v(t) dt$$

and the result for  $C(t)$  follows from equation (5), with  $C_J(t) = -\sigma_{1,J} \eta_{1,J} \mathbb{V}ar(J_{1,-}(1)) v(t)$ .

In this setting, the characteristic function of the process  $X(t)$  driving the log-returns can be recovered in two alternative ways. The first one is by means of the change of measure of Carr and Wu (2004) reviewed in Section 2; the second one is by means of standard results on affine processes as in Kallsen (2006). In what follows, we assume that all the admissibility conditions in Kallsen (2006) are satisfied.

**Proof of Proposition 1.** The change of measure argument relies on two key observations. Firstly, in order to recover the relevant dynamics of  $X(t)$  it suffices to consider the dynamics of the base Lévy process by applying the random time transformations  $v(t)$  where required (see Küchler and Sørensen, 1997, Jacod, 1979, for example). Secondly, the  $\mathbb{M}$ -measure is an Esscher-type probability measure, which implies that the characteristic exponent of the base processes satisfies equation (6). Thus.

- i) The Girsanov theorem implies that  $W_1(t) - iu\sigma_{1,D}t$  is a  $\mathbb{M}$ -Brownian motion, and  $\partial\Pi(J_j|\mathbb{M}) = (\alpha_j^{\mathbb{M}}, 0, \nu_j^{\mathbb{M}}(dx))$  for

$$\begin{aligned} \alpha_j^{\mathbb{M}} &= \alpha_{j,+} + \int_{\mathbb{R}} x 1_{|x| \leq 1} (e^{iu\sigma_{j,J}x} - 1) \nu_{j,+}(dx) + \alpha_{j,-} + \int_{\mathbb{R}} x 1_{|x| \leq 1} (e^{iu\sigma_{j,J}x} - 1) \nu_{j,-}(dx) \\ &= \alpha_{j,+}^{\mathbb{M}} + \alpha_{j,-}^{\mathbb{M}}, \\ \nu_j^{\mathbb{M}}(dx) &= e^{iu\sigma_{j,J}x} \nu_j(dx), \quad j = 0, 1. \end{aligned}$$

For an illustration, let us consider the case of the CGMY process of Carr et al. (2002). The CGMY process is a Lévy process described by the Lévy measure

$$\nu(x) = C \left( \frac{e^{-G|x|}}{|x|^{1+Y}} 1_{x < 0} + \frac{e^{-Mx}}{x^{1+Y}} 1_{x > 0} \right),$$

for  $C > 0$ ,  $G \geq 0$ ,  $M \geq 0$ ,  $Y < 2$ ; the corresponding characteristic exponent is

$$\varphi(u) = C\Gamma(-Y) \left( (G + iu)^Y - G^Y + (M - iu)^Y - M^Y \right),$$

see Carr et al. (2002). It follows that

$$\nu^{\mathbb{M}}(x) = C \left( \frac{e^{-(G+iu\sigma_{\cdot,J})|x|}}{|x|^{1+Y}} 1_{x<0} + \frac{e^{-(M-iu\sigma_{\cdot,J})x}}{x^{1+Y}} 1_{x>0} \right).$$

In other words, the parameters affected by the change of measure are the parameters  $G$  and  $M$ ; specifically, under the leverage neutral measure the CGMY process has parameters  $C, G^{\mathbb{M}}, M^{\mathbb{M}}, Y$  for  $G^{\mathbb{M}} = G + iu\sigma_{\cdot,J}$  and  $M^{\mathbb{M}} = M - iu\sigma_{\cdot,J}$ . The characteristic exponent of the process of the negative jumps follows directly.

- ii) The  $\mathbb{M}$ -dynamics of the process  $Y_j(t)$ ,  $j = 0, 1$ , follows from Proposition 4 in Ballotta et al. (2017) due to the factor construction in place. In details, we first observe that in the present setup the loading coefficient applied to the diffusion part of  $Y_1(t)$  is  $\rho$ , therefore  $Z_1(t) - iu\sigma_{1,D}\rho t$  is the  $\mathbb{M}$ -Brownian motion driving  $Y_1(t)$ . Further, the loading coefficient applied to the pure jump part of  $Y_j(t)$  is  $-\eta_{j,J}$ ,  $j = 0, 1$ . ■

**Proof of Proposition 2.** The required characteristic function of  $T(t)$  can be recovered by observing that  $(v(t), T(t))$  are bivariate affine; consequently

$$\mathbb{E}^{\mathbb{M}} \left( e^{i w v(t) + i z T(t)} \right) = e^{\Psi_0(w, z; t) + \Psi_1(w, z; t) v(0)},$$

with the affine exponents  $\Psi_0, \Psi_1$  solutions to the system of Riccati-type ODEs

$$\begin{aligned} \Psi'_0(w, z; t) &= \kappa\theta\Psi_1(w, z; t) + \varphi_{j_0}^{\mathbb{M}}(i\eta_{0,J}\Psi_1(w, z; t)), \\ \Psi_0(w, z; 0) &= 0 \end{aligned} \tag{A.1}$$

$$\begin{aligned} \Psi'_1(w, z; t) &= iz - \kappa^{\mathbb{M}}\Psi_1(w, z; t) + \frac{\eta_{1,D}^2}{2}\Psi_1^2(w, z; t) + \varphi_{j_1}^{\mathbb{M}}(i\eta_{1,J}\Psi_1(w, z; t)), \\ \Psi_1(w, z; 0) &= iw. \end{aligned} \tag{A.2}$$

The required characteristic exponents under the probability measure  $\mathbb{M}$  follow from Proposition 1. Equations (20)–(21) follow by setting  $w = 0, z = -i\varphi_{L_1}(u)$ , and noting that  $A(t) = \varphi_{L_0}(u)t + \Psi_0(0, u; t)$  and  $B(t) = \Psi_1(0, u; t)$ .

We now use the argument based on the theory of affine processes, and show how the two approaches can be reconciled leading to the same system of ODEs for the affine exponents. Under the given assumptions, the characteristic function of the bivariate affine process  $(v(t), X(t))$  is

$$\mathbb{E} \left( e^{i w v(t) + i u X(t)} \right) = e^{\Phi_0(w, u; t) + \Phi_1(w, u; t) v(0)}$$

with the affine exponents  $\Phi_0, \Phi_1$  solutions to the system of Riccati-type ODEs

$$\begin{aligned} \Phi'_0(w, u; t) &= (\kappa\theta - \eta_{0,J}\tilde{\alpha}_0)\Phi_1(w, u; t) - iu(\varphi_0(-i) - \sigma_{0,J}\alpha_0) \\ &\quad + \int_{\mathbb{R}^+ \times \mathbb{R}} \left( e^{-\Phi_1(w, u; t)\eta_{0,J}y + iu\sigma_{0,J}x} - 1 + (\Phi_1(w, u; t)\eta_{0,J}y - iu\sigma_{0,J}x) 1_{y^2+x^2 \leq 1} \right) K_0(dy \times dx), \\ \Phi_0(w, u; 0) &= 0 \\ \Phi'_1(w, u; t) &= -(\kappa + \eta_{1,J}\tilde{\alpha}_1 - iu\eta_{1,D}\sigma_{1,D}\rho)\Phi_1(w, u; t) - iu(\varphi_1(-i) - \sigma_{1,J}\alpha_1) - \frac{\sigma_{1,D}^2}{2}u^2 + \frac{\eta_{1,D}^2}{2}\Phi_1^2(w, u; t) \\ &\quad + \int_{\mathbb{R}^+ \times \mathbb{R}} \left( e^{-\Phi_1(w, u; t)\eta_{1,J}y + iu\sigma_{1,J}x} - 1 + (\Phi_1(w, u; t)\eta_{1,J}y - iu\sigma_{1,J}x) 1_{y^2+x^2 \leq 1} \right) K_1(dy \times dx), \\ \Phi_1(w, u; 0) &= iw. \end{aligned}$$

The characteristic function of the process  $X(t)$  follows by setting  $w = 0$ .

In order to reconcile this system of ODEs with equations (20)–(21), we use equation (13) to rewrite the above system of ODEs under the  $\mathbb{P}$  measure as

$$\begin{aligned}\Phi'_0(w, u; t) &= \kappa\theta\Phi_1(w, u; t) + \varphi_{L_0}(u) - \varphi_{J_{0,+}}(u\sigma_{0,J}) - \varphi_{J_{0,-}}(u\sigma_{0,J}) \\ &\quad + \varphi_{(\tilde{J}_0, J_0)}(i\eta_{0,J}\Phi_1(w, u; t), u\sigma_{0,J})\end{aligned}\tag{A.3}$$

$$\Phi_0(w, u; 0) = 0$$

$$\begin{aligned}\Phi'_1(w, u; t) &= -(\kappa - iu\eta_{1,D}\sigma_{1,D}\rho)\Phi_1(w, u; t) + \varphi_{L_1}(u) - \varphi_{J_{1,+}}(u\sigma_{1,J}) - \varphi_{J_{1,-}}(u\sigma_{1,J}) \\ &\quad + \frac{\eta_{1,D}^2}{2}\Phi_1^2(w, u; t) + \varphi_{(\tilde{J}_1, J_1)}(i\eta_{1,J}\Phi_1(w, u; t), u\sigma_{1,J}),\end{aligned}\tag{A.4}$$

$$\Phi_1(w, u; 0) = iw.$$

$\varphi_{(\tilde{J}, J)}$  denotes the joint characteristic exponent of the bivariate pure jump Lévy process  $(\tilde{J}, J)$ . Bearing in mind that the factor construction in place in this paper requires only one source of systematic risk, the following cases are pertinent to our setting.

Case I  $\tilde{J}_0(t) = J_{0,-}(t)$ ;  $\tilde{J}_1(t), J_1(t)$  independent. Then, from Ballotta and Bonfiglioli (2014)

$$\begin{aligned}\varphi_{(\tilde{J}_0, J_0)}(w, z) &= \varphi_{J_{0,-}}(w+z) + \varphi_{J_{0,+}}(z) = \varphi_{\tilde{J}_0}(w+z) + \varphi_{J_{0,+}}(z) \\ \varphi_{(\tilde{J}_1, J_1)}(w, z) &= \varphi_{\tilde{J}_1}(w) + \varphi_{J_{1,+}}(z) + \varphi_{J_{1,-}}(z).\end{aligned}$$

After substitution in (A.3)–(A.4), equation (19) with  $\sigma_{l,J} = \sigma_{0,J}$  leads to

$$\begin{aligned}\Phi'_0(w, u; t) &= \varphi_{L_0}(u) + \kappa\theta\Phi_1(w, u; t) + \varphi_{\tilde{J}_0}^{\mathbb{M}}(i\eta_{0,J}\Phi_1(w, u; t)), \\ \Phi_0(w, u; 0) &= 0 \\ \Phi'_1(w, u; t) &= \varphi_{L_1}(u) - (\kappa - iu\eta_{1,D}\sigma_{1,D}\rho)\Phi_1(w, u; t) + \frac{\eta_{1,D}^2}{2}\Phi_1^2(w, u; t) \\ &\quad + \varphi_{\tilde{J}_1}^{\mathbb{M}}(-i\eta_{1,J}\Phi_1(w, u; t)), \\ \Phi_1(w, u; 0) &= iw.\end{aligned}$$

Equations (20)–(21) follow bearing in mind the definition of  $k^{\mathbb{M}}$ , and setting  $w = 0$ ,  $A(t) = \Phi_0(0, u; t)$ ,  $B(t) = \Phi_1(0, u; t)$ .

Case II  $\tilde{J}_0(t) = J_{1,-}(t)$ ;  $\tilde{J}_1(t), J_1(t)$  independent. Then, from Ballotta and Bonfiglioli (2014)

$$\begin{aligned}\varphi_{(\tilde{J}_0, J_0)}(w, z) &= \varphi_{J_{1,-}}(w) + \varphi_{J_{0,+}}(z) + \varphi_{J_{0,-}}(z) = \varphi_{\tilde{J}_0}(w) + \varphi_{J_{0,+}}(z) + \varphi_{J_{0,-}}(z) \\ \varphi_{(\tilde{J}_1, J_1)}(w, z) &= \varphi_{\tilde{J}_1}(w) + \varphi_{J_{1,+}}(z) + \varphi_{J_{1,-}}(z).\end{aligned}$$

As equation (6) implies  $\tilde{\varphi}_0(w) = \tilde{\varphi}_0^{\mathbb{M}}(w)$ , equations (20)–(21) follow from the same argument as in Case I.

Case III  $\tilde{J}_0(t), J_0(t)$  independent;  $\tilde{J}_1(t) = J_{0,-}(t)$ . Then, from Ballotta and Bonfiglioli (2014)

$$\begin{aligned}\varphi_{(\tilde{J}_0, J_0)}(w, z) &= \varphi_{\tilde{J}_0}(w) + \varphi_{J_{0,+}}(z) + \varphi_{J_{0,-}}(z) \\ \varphi_{(\tilde{J}_1, J_1)}(w, z) &= \varphi_{J_{0,-}}(w) + \varphi_{J_{1,+}}(z) + \varphi_{J_{1,-}}(z) = \varphi_{\tilde{J}_1}(w) + \varphi_{J_{1,+}}(z) + \varphi_{J_{1,-}}(z).\end{aligned}$$

The required result follows from the same argument as in the previous cases.

Case IV  $\tilde{J}_0(t), J_0(t)$  independent;  $\tilde{J}_1(t) = J_{1,-}(t)$ . Then, from Ballotta and Bonfiglioli (2014)

$$\begin{aligned}\varphi_{(\tilde{J}_0, J_0)}(w, z) &= \varphi_{\tilde{J}_0}(w) + \varphi_{J_0,+}(z) + \varphi_{J_0,-}(z) \\ \varphi_{(\tilde{J}_1, J_1)}(w, z) &= \varphi_{J_{1,-}}(w+z) + \varphi_{J_{1,+}}(z) = \varphi_{\tilde{J}_1}(w+z) + \varphi_{J_{1,+}}(z).\end{aligned}$$

The required result follows from the same argument as above for  $\sigma_{l,J} = \sigma_{1,J}$ . ■

**Proof of Proposition 3** The argument is based on conditioning, the Bayes formula and the Doob's optional stopping theorem.

$$\begin{aligned}\phi_X(u; s, t) &= \mathbb{E} \left[ \mathbb{E}_s \left( e^{iu(L_0(t) - L_0(s) + L_1(T(t)) - L_1(T(s)))} \right) \right] \\ &= e^{\varphi_{L_0}(u)(t-s)} \mathbb{E} \left[ M_u(s)^{-1} \mathbb{E}_s (M_u(s)) \mathbb{E}_s^{\mathbb{M}} \left( e^{\varphi_{L_1}(u)(T(t) - T(s))} \right) \right] \\ &= e^{\varphi_{L_0}(u)(t-s)} \mathbb{E} \left[ \mathbb{E}_s^{\mathbb{M}} \left( e^{\varphi_{L_1}(u)(T(t) - T(s))} \right) \right].\end{aligned}$$

From the proof of Proposition 2, it follows that

$$\phi_X(u; s, t) = e^{A(t-s)} \mathbb{E} \left( e^{B(t-s)v(s)} \right) \quad (\text{A.5})$$

Notice that now expectations are to be taken under the risk neutral martingale measure  $\mathbb{P}$ . Solution to (A.5) follows from the fact that the activity rate is affine. ■

## B Option Data

For the purpose of the empirical investigation, we use daily closing bid and ask quotes of standard European options on the S&P500 index across different strikes and maturities. The data sets contain matching spot prices (index level) and interest rates corresponding to each option quote. By means of the put-call parity we recover the (implied) forward prices. We apply the following filters to the data: time to maturity greater than five business days, strictly positive bid option price, ask price no less than the bid price. After applying these filters, we also plot the mid-implied volatility quote for each day and maturity against strike prices to visually check for and remove the obvious outliers. These filtering rules follow Huang and Wu (2004). Finally, we only use out-of-the-money call and put options.

For the Calibration Exercise 1, the option quotes are observed on April 24th 2017 on the Bloomberg platform; we build the full volatility surface using the SVI methodology of Gatheral and Jacquier (2014) for a total of 1,573 points. The maturities of the option contracts range from 25 to 970 business days; finally, we use the same range of strikes for all maturities ranging from 0.85 to 1.25. We summarize the data set in Table B.1, which reports in panel A the number of option contracts per each category of maturities and moneyness,  $S/K$ , in panel B the average option price in each category, and in panel C the average Black-Scholes implied volatility in each category.

For the Calibration Exercise 2, instead, we use quotes from OptionMetrics covering the period September 4th 2012 to August 27th 2014, i.e. a period of time non overlapping with the one chosen

for the 1 day calibration. In addition to the filters described above, we only refer to Wednesday's quotes, and restrict our attention to the more liquid options with moneyness between 0.83 and 1.49. Maturities in this case span from 5 to 1031 business days; Table B.2 summarizes the data according to the same moneyness/day to maturity categories as above. We use the first year of data (20,525 contracts) to estimate the parameters of the models considered in the previous sections, and then the remaining year of data (18,066 contracts) to test the reliability of the performance of the models.

	DTM < 30	30 < DTM < 90	90 < DTM < 180	DTM > 180	All
PANEL A: Number of Option contracts					
$S/K < 0.975$	36	72	72	216	396
$0.975 < S/K < 1$	12	24	24	72	132
$1 < S/K/1.025$	12	24	24	72	132
$1.025 < S/K < 1.05$	11	22	22	66	121
$1.05 < S/K < 1.075$	10	20	20	60	110
$S/K > 1.075$	62	124	124	372	682
All	143	286	286	858	1573
PANEL B: Average Option Price					
$S/K < 0.975$	0.48	3.36	9.21	66.92	38.83
$0.975 < S/K < 1$	10.72	26.42	43.64	122.80	80.69
$1 < S/K/1.025$	15.06	33.31	53.92	136.59	91.73
$1.025 < S/K < 1.05$	6.48	20.42	38.67	117.55	75.45
$1.05 < S/K < 1.075$	3.73	13.92	29.10	102.17	63.89
$S/K > 1.075$	1.26	5.68	13.61	65.68	39.44
All	3.59	10.86	21.41	83.27	51.62
PANEL C: Average Option Implied Volatility					
$S/K < 0.975$	10.72%	8.88%	8.83%	11.88%	10.67%
$0.975 < S/K < 1$	8.71%	9.50%	10.37%	13.38%	11.70%
$1 < S/K/1.025$	10.64%	11.01%	11.66%	14.14%	12.80%
$1.025 < S/K < 1.05$	13.47%	12.77%	13.02%	14.90%	14.04%
$1.05 < S/K < 1.075$	16.40%	14.54%	14.33%	15.61%	15.25%
$S/K > 1.075$	26.27%	20.83%	18.92%	18.13%	19.51%
All	17.90%	14.99%	14.28%	15.40%	15.35%

Table B.1: S&P500 Option Data - Calibration Exercise 1. Spot value: 2,372.81. Observation date: 24/04/2017. Source Bloomberg. Implied volatilities extracted using the Black-Scholes formula.

	SUBSET 1						SUBSET 2				
	DTM<30	30<DTM<90	90<DTM<180	DTM>180	All		DTM<30	30<DTM<90	90<DTM<180	DTM>180	All
	PANEL A: Number of Option contracts						PANEL A: Number of Option contracts				
$S/K < 0.975$	655	2007	805	888	4355	$S/K < 0.975$	445	1578	784	686	3493
$0.975 < S/K < 1$	1192	1015	246	202	2655	$0.975 < S/K < 1$	1179	282	207	199	1867
$1 < S/K < 1.025$	1156	957	260	216	2589	$1 < S/K < 1.025$	1292	556	116	209	2173
$1.025 < S/K < 1.05$	1081	847	187	147	2262	$1.025 < S/K < 1.05$	1124	805	78	165	2172
$1.05 < S/K < 1.075$	827	858	194	143	2022	$1.05 < S/K < 1.075$	809	897	65	149	1920
$S/K > 1.075$	772	3396	1317	1157	6642	$S/K > 1.075$	1275	3637	841	688	6441
All	5683	9080	3009	2753	20525	All	6124	7755	2091	2096	18066
	PANEL B: Average Option Price						PANEL B: Average Option Price				
$S/K < 0.975$	1.87	4.61	10.52	28.74	10.21	$S/K < 0.975$	1.34	3.22	9.14	32.73	10.10
$0.975 < S/K < 1$	7.89	18.78	36.41	77.36	19.98	$0.975 < S/K < 1$	7.10	22.70	39.01	82.09	20.99
$1 < S/K < 1.025$	10.80	25.10	47.28	91.83	26.51	$1 < S/K < 1.025$	10.02	22.35	54.98	105.30	24.74
$1.025 < S/K < 1.05$	4.41	15.21	35.85	84.42	16.25	$1.025 < S/K < 1.05$	3.73	11.82	42.99	93.69	14.97
$1.05 < S/K < 1.075$	2.34	9.62	27.14	71.91	12.73	$1.05 < S/K < 1.075$	2.18	7.21	33.84	77.80	11.47
$S/K > 1.075$	1.42	3.83	9.22	36.70	10.35	$S/K > 1.075$	1.18	3.36	6.59	42.25	7.50
All	5.44	9.52	17.89	45.82	14.49	All	4.79	6.72	15.65	55.78	12.79
	PANEL C: Average Option Implied Volatility						PANEL C: Average Option Implied Volatility				
$S/K < 0.975$	11.89%	11.37%	12.16%	13.83%	12.10%	$S/K < 0.975$	11.99%	10.68%	10.79%	12.59%	11.25%
$0.975 < S/K < 1$	11.98%	12.45%	13.78%	15.91%	12.62%	$0.975 < S/K < 1$	9.89%	13.12%	12.61%	14.35%	11.15%
$1 < S/K < 1.025$	14.12%	14.03%	14.77%	16.60%	14.36%	$1 < S/K < 1.025$	11.67%	13.45%	14.16%	15.31%	12.61%
$1.025 < S/K < 1.05$	16.84%	15.67%	16.24%	17.44%	16.39%	$1.025 < S/K < 1.05$	14.57%	14.61%	15.66%	15.95%	14.73%
$1.05 < S/K < 1.075$	19.57%	17.30%	17.23%	17.97%	18.27%	$1.05 < S/K < 1.075$	18.30%	16.23%	17.13%	16.62%	17.16%
$S/K > 1.075$	23.04%	22.05%	22.79%	22.29%	22.35%	$S/K > 1.075$	25.07%	21.47%	23.12%	20.39%	22.28%
All	15.93%	16.73%	17.75%	18.17%	16.85%	All	15.55%	17.08%	16.50%	16.14%	16.38%

Table B.2: S&P500 Option Data - Calibration Exercise 2. Subset 1 Observation period: 4/09/2012 - 28/08/2013. Subset 2 Observation period: 4/09/2013 - 27/08/2014. Source OptionMetrics. Implied volatilities extracted using the Black-Scholes formula.

## C Further Results

		1 SV Factor Model							2 SV Factor Model					
Moneyness $S/K$	Model	Days-to-Maturity					Moneyness $S/K$	Model	Days-to-Maturity					
		<30	30 - 90	90 - 180	>180	All			<30	30 - 90	90 - 180	>180	All	
<0.975	Heston	0.0188	0.0058	0.0060	0.0045	0.0075	<0.975	Heston	0.0232	0.0056	0.0017	0.0013	0.0075	
	JH	0.0098	0.0051	0.0027	0.0010	0.0039		SVFSE	0.0076	0.0041	0.0022	0.0007	0.0031	
	JBNS	0.0076	0.0077	0.0046	0.0072	0.0069		SVFHOU	0.0077	0.0050	0.0023	0.0021	0.0037	
	SVFSE	0.0068	0.0037	0.0020	0.0010	0.0028								
	SVFHOU	0.0049	0.0029	0.0019	0.0016	0.0024								
0.975 - 1	Heston	0.0146	0.0074	0.0012	0.0047	0.0065	0.975 - 1	Heston	0.0030	0.0019	0.0005	0.0008	0.0014	
	JH	0.0025	0.0018	0.0007	0.0010	0.0013		SVFSE	0.0041	0.0026	0.0002	0.0007	0.0018	
	JBNS	0.0270	0.0177	0.0063	0.0045	0.0119		SVFHOU	0.0106	0.0059	0.0007	0.0018	0.0043	
	SVFSE	0.0022	0.0017	0.0010	0.0009	0.0013								
	SVFHOU	0.0006	0.0013	0.0003	0.0008	0.0008								
1 - 1.025	Heston	0.0044	0.0033	0.0036	0.0052	0.0046	1 - 1.025	Heston	0.0070	0.0023	0.0008	0.0007	0.0024	
	JH	0.0024	0.0013	0.0008	0.0010	0.0012		SVFSE	0.0014	0.0012	0.0002	0.0008	0.0009	
	JBNS	0.0179	0.0106	0.0037	0.0033	0.0076		SVFHOU	0.0037	0.0021	0.0010	0.0019	0.0020	
	SVFSE	0.0032	0.0014	0.0007	0.0009	0.0013								
	SVFHOU	0.0018	0.0013	0.0010	0.0010	0.0011								
1.025 - 1.05	Heston	0.0044	0.0067	0.0060	0.0058	0.0059	1.025 - 1.05	Heston	0.0075	0.0029	0.0004	0.0008	0.0027	
	JH	0.0018	0.0009	0.0007	0.0010	0.0010		SVFSE	0.0017	0.0015	0.0004	0.0008	0.0010	
	JBNS	0.0029	0.0034	0.0018	0.0021	0.0024		SVFHOU	0.0061	0.0027	0.0016	0.0019	0.0027	
	SVFSE	0.0021	0.0009	0.0005	0.0009	0.0010								
	SVFHOU	0.0044	0.0012	0.0012	0.0015	0.0019								
1.05 - 1.075	Heston	0.0046	0.0067	0.0060	0.0058	0.0059	1.05 - 1.075	Heston	0.0054	0.0029	0.0004	0.0010	0.0022	
	JH	0.0018	0.0009	0.0007	0.0010	0.0010		SVFSE	0.0008	0.0019	0.0004	0.0009	0.0011	
	JBNS	0.0029	0.0034	0.0018	0.0021	0.0024		SVFHOU	0.0068	0.0033	0.0018	0.0018	0.0029	
	SVFSE	0.0021	0.0009	0.0005	0.0009	0.0010								
	SVFHOU	0.0044	0.0012	0.0012	0.0015	0.0019								
>1.075	Heston	0.0026	0.0087	0.0074	0.0062	0.0067	>1.075	Heston	0.0191	0.0027	0.0013	0.0014	0.0060	
	JH	0.0017	0.0006	0.0005	0.0010	0.0010		SVFSE	0.0024	0.0015	0.0007	0.0010	0.0012	
	JBNS	0.0052	0.0010	0.0009	0.0016	0.0021		SVFHOU	0.0026	0.0051	0.0019	0.0019	0.0028	
	SVFSE	0.0004	0.0004	0.0004	0.0009	0.0008								
	SVFHOU	0.0041	0.0012	0.0010	0.0018	0.0019								
All	Heston	0.0026	0.0087	0.0074	0.0062	0.0067	All	Heston	0.0175	0.0036	0.0012	0.0012	0.0056	
	JH	0.0017	0.0006	0.0005	0.0010	0.0010		SVFSE	0.0043	0.0025	0.0012	0.0009	0.0019	
	JBNS	0.0052	0.0010	0.0009	0.0016	0.0021		SVFHOU	0.0059	0.0047	0.0018	0.0020	0.0031	
	SVFSE	0.0004	0.0004	0.0004	0.0009	0.0008								
	SVFHOU	0.0041	0.0012	0.0010	0.0018	0.0019								
>1.075	Heston	0.0291	0.0070	0.0080	0.0074	0.0113	>1.075	Heston	0.0191	0.0027	0.0013	0.0014	0.0060	
	JH	0.0031	0.0015	0.0012	0.0012	0.0015		SVFSE	0.0024	0.0015	0.0007	0.0010	0.0012	
	JBNS	0.0121	0.0028	0.0026	0.0066	0.0063		SVFHOU	0.0026	0.0051	0.0019	0.0019	0.0028	
	SVFSE	0.0018	0.0013	0.0013	0.0011	0.0013								
	SVFHOU	0.0040	0.0017	0.0019	0.0017	0.0021								
All	Heston	0.0218	0.0066	0.0067	0.0062	0.0090	All	Heston	0.0175	0.0036	0.0012	0.0012	0.0056	
	JH	0.0054	0.0029	0.0016	0.0011	0.0023		SVFSE	0.0043	0.0025	0.0012	0.0009	0.0019	
	JBNS	0.0130	0.0074	0.0036	0.0059	0.0068		SVFHOU	0.0059	0.0047	0.0018	0.0020	0.0031	
	SVFSE	0.0038	0.0022	0.0014	0.0010	0.0018								
	SVFHOU	0.0040	0.0020	0.0016	0.0016	0.0020								

Table C.1: IVRMSE by moneyness and days to maturity. Data: S&P500 options. Observation date: 24/04/2017. Base process: CGMY. Repricing: parameter set in Table 3.

Moneyness S/K	Model	IN SAMPLE					OUT OF SAMPLE				
		Days-to-Maturity					Days-to-Maturity				
		< 30	30 - 90	90 - 180	>180	All	< 30	30 - 90	90 - 180	>180	All
<0.975	Heston	0.0084	0.0063	0.0066	0.0089	0.0073	0.0194	0.0088	0.0106	0.0141	0.0121
	JH	0.0078	0.0073	0.0067	0.0073	0.0073	0.0133	0.0093	0.0077	0.0116	0.0101
	JBNS	0.0435	0.0302	0.0356	0.0312	0.0337	0.0102	0.0113	0.0155	0.0289	0.0170
	SVFSE	0.0089	0.0061	0.0067	0.0077	0.0070	0.0251	0.0106	0.0085	0.0157	0.0140
	SVFHOU	0.0104	0.0092	0.0115	0.0103	0.0101	0.0125	0.0099	0.0088	0.0138	0.0109
0.975 - 1	Heston	0.0069	0.0047	0.0057	0.0105	0.0064	0.0097	0.0093	0.0077	0.0121	0.0097
	JH	0.0070	0.0048	0.0045	0.0089	0.0062	0.0062	0.0059	0.0057	0.0111	0.0068
	JBNS	0.0292	0.0138	0.0120	0.0139	0.0220	0.0158	0.0147	0.0158	0.0222	0.0164
	SVFSE	0.0079	0.0059	0.0060	0.0097	0.0072	0.0107	0.0084	0.0084	0.0155	0.0108
	SVFHOU	0.0126	0.0095	0.0106	0.0110	0.0112	0.0097	0.0106	0.0077	0.0133	0.0101
1 - 1.025	Heston	0.0073	0.0051	0.0057	0.0107	0.0068	0.0101	0.0088	0.0081	0.0105	0.0097
	JH	0.0091	0.0046	0.0046	0.0084	0.0073	0.0049	0.0050	0.0051	0.0104	0.0057
	JBNS	0.0226	0.0132	0.0113	0.0168	0.0181	0.0145	0.0128	0.0139	0.0183	0.0144
	SVFSE	0.0102	0.0069	0.0071	0.0097	0.0088	0.0110	0.0104	0.0083	0.0154	0.0112
	SVFHOU	0.0147	0.0093	0.0100	0.0109	0.0122	0.0076	0.0093	0.0083	0.0138	0.0089
1.025 - 1.05	Heston	0.0110	0.0049	0.0057	0.0119	0.0089	0.0106	0.0080	0.0078	0.0100	0.0096
	JH	0.0097	0.0037	0.0049	0.0091	0.0076	0.0060	0.0041	0.0045	0.0100	0.0058
	JBNS	0.0149	0.0108	0.0132	0.0207	0.0139	0.0224	0.0142	0.0117	0.0152	0.0189
	SVFSE	0.0112	0.0069	0.0082	0.0104	0.0095	0.0122	0.0092	0.0067	0.0153	0.0113
	SVFHOU	0.0157	0.0092	0.0115	0.0123	0.0131	0.0091	0.0076	0.0080	0.0137	0.0090
1.05 - 1.075	Heston	0.0187	0.0053	0.0052	0.0112	0.0129	0.0244	0.0070	0.0060	0.0096	0.0168
	JH	0.0095	0.0041	0.0044	0.0085	0.0072	0.0104	0.0042	0.0036	0.0088	0.0078
	JBNS	0.0149	0.0107	0.0121	0.0262	0.0142	0.0214	0.0157	0.0084	0.0128	0.0180
	SVFSE	0.0115	0.0077	0.0070	0.0095	0.0095	0.0138	0.0093	0.0065	0.0145	0.0118
	SVFHOU	0.0151	0.0097	0.0104	0.0108	0.0123	0.0128	0.0072	0.0070	0.0130	0.0104
>1.075	Heston	0.0266	0.0080	0.0066	0.0139	0.0125	0.0546	0.0145	0.0097	0.0078	0.0270
	JH	0.0106	0.0060	0.0062	0.0105	0.0076	0.0168	0.0081	0.0061	0.0070	0.0101
	JBNS	0.0145	0.0149	0.0259	0.0344	0.0219	0.0177	0.0142	0.0160	0.0176	0.0156
	SVFSE	0.0134	0.0096	0.0092	0.0117	0.0104	0.0165	0.0110	0.0107	0.0136	0.0125
	SVFHOU	0.0162	0.0119	0.0138	0.0144	0.0133	0.0171	0.0103	0.0085	0.0108	0.0118
All	Heston	0.0141	0.0066	0.0063	0.0117	0.0099	0.0280	0.0117	0.0096	0.0112	0.0187
	JH	0.0090	0.0057	0.0059	0.0091	0.0073	0.0103	0.0074	0.0066	0.0098	0.0087
	JBNS	0.0246	0.0186	0.0260	0.0301	0.0233	0.0178	0.0138	0.0154	0.0220	0.0165
	SVFSE	0.0105	0.0078	0.0080	0.0101	0.0090	0.0142	0.0104	0.0093	0.0149	0.0123
	SVFHOU	0.0143	0.0104	0.0123	0.0124	0.0121	0.0118	0.0096	0.0084	0.0128	0.0107

Table C.2: IVRMSE by moneyness and days to maturity. In/Out of Sample analysis. 1 Stochastic Volatility Factor models. Data: S&P500 options. Observation period: 4/09/2012 - 29/08/2014. Source: OptionMetrics. Base process: CGMY.

Moneyness $S/K$	Model	IN SAMPLE					OUT OF SAMPLE				
		Days-to-Maturity					Days-to-Maturity				
		< 30	30 - 90	90 - 180	>180	All	< 30	30-90	90 - 180	>180	All
< 0.975	Heston	0.0080	0.0066	0.0058	0.0077	0.0069	0.0135	0.0089	0.0069	0.0140	0.0104
	SVFSE	0.0069	0.0071	0.0071	0.0071	0.0071	0.0091	0.0080	0.0064	0.0097	0.0082
	SVFHOU	0.0087	0.0064	0.0060	0.0081	0.0071	0.0125	0.0066	0.0063	0.0148	0.0096
0.975 - 1	Heston	0.0067	0.0039	0.0039	0.0099	0.0059	0.0063	0.0076	0.0052	0.0145	0.0077
	SVFSE	0.0072	0.0047	0.0049	0.0084	0.0063	0.0054	0.0047	0.0045	0.0083	0.0056
	SVFHOU	0.0065	0.0037	0.0042	0.0104	0.0058	0.0061	0.0051	0.0072	0.0156	0.0077
1 - 1.025	Heston	0.0067	0.0045	0.0037	0.0094	0.0060	0.0056	0.0066	0.0056	0.0142	0.0071
	SVFSE	0.0097	0.0051	0.0045	0.0076	0.0076	0.0045	0.0047	0.0037	0.0083	0.0050
	SVFHOU	0.0076	0.0043	0.0043	0.0100	0.0065	0.0050	0.0045	0.0075	0.0150	0.0067
1.025 - 1.05	Heston	0.0068	0.0036	0.0039	0.0088	0.0058	0.0069	0.0048	0.0055	0.0133	0.0069
	SVFSE	0.0100	0.0042	0.0043	0.0081	0.0078	0.0057	0.0033	0.0032	0.0083	0.0051
	SVFHOU	0.0075	0.0034	0.0044	0.0099	0.0063	0.0065	0.0031	0.0070	0.0146	0.0066
1.05 - 1.075	Heston	0.0111	0.0037	0.0044	0.0090	0.0080	0.0150	0.0044	0.0054	0.0124	0.0108
	SVFSE	0.0084	0.0043	0.0039	0.0076	0.0065	0.0087	0.0035	0.0027	0.0070	0.0065
	SVFHOU	0.0058	0.0039	0.0042	0.0098	0.0053	0.0128	0.0042	0.0053	0.0136	0.0096
>1.075	Heston	0.0151	0.0055	0.0076	0.0113	0.0087	0.0345	0.0076	0.0066	0.0090	0.0168
	SVFSE	0.0068	0.0054	0.0073	0.0094	0.0068	0.0118	0.0071	0.0061	0.0067	0.0081
	SVFHOU	0.0055	0.0061	0.0072	0.0112	0.0074	0.0196	0.0117	0.0059	0.0102	0.0130
All	Heston	0.0091	0.0052	0.0062	0.0098	0.0073	0.0177	0.0073	0.0065	0.0125	0.0123
	SVFSE	0.0084	0.0055	0.0065	0.0083	0.0070	0.0078	0.0064	0.0058	0.0082	0.0071
	SVFHOU	0.0070	0.0054	0.0061	0.0100	0.0067	0.0115	0.0089	0.0063	0.0135	0.0102

Table C.3: IVRMSE by moneyness and days to maturity. In/Out of Sample analysis. 2 Stochastic Volatility Factor models. Data S&P500 options. Observation period: 4/09/2012 - 29/08/2014. Source: OptionMetrics. Base process: CGMY.

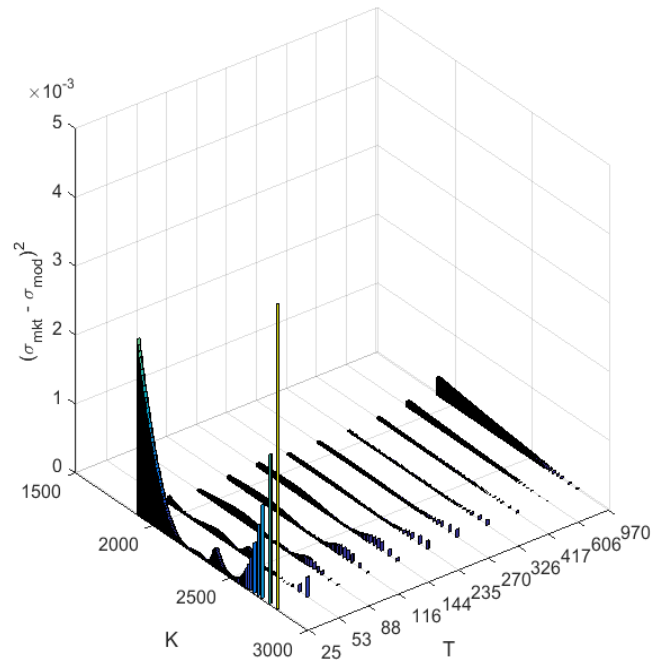


Figure C.1: Heston model calibration performance: 1-Day Calibration. Metrics: squared errors in volatility.  $\sigma_{mod}$ : model implied volatility.  $\sigma_{mkt}$ : market implied volatility. Spot value: 2,372.81. Data: S&P500 options observed on 24/04/2017. Source Bloomberg.

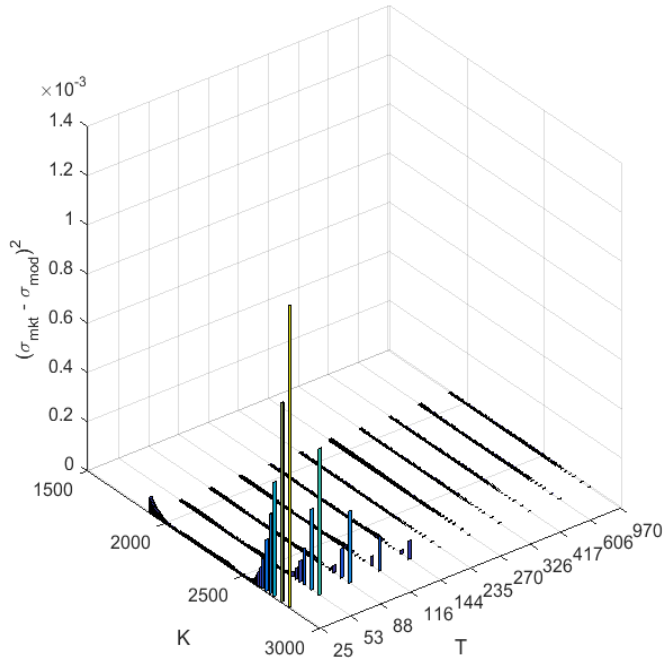


Figure C.2: JH model calibration performance: 1-Day Calibration. Metrics: squared errors in volatility.  $\sigma_{mod}$ : model implied volatility.  $\sigma_{mkt}$ : market implied volatility. Spot value: 2,372.81. Data: S&P500 options observed on 24/04/2017. Source Bloomberg.

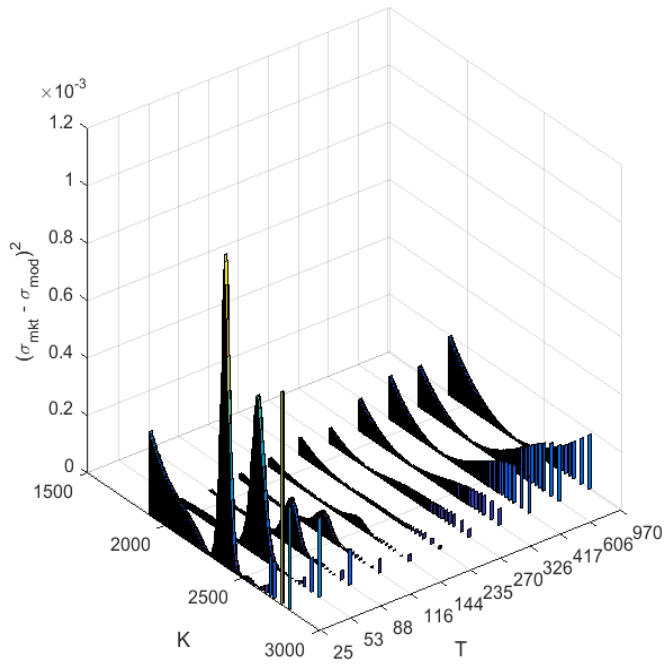


Figure C.3: JBNS model calibration performance: 1-Day Calibration. Metrics: squared errors in volatility.  $\sigma_{mod}$ : model implied volatility.  $\sigma_{mkt}$ : market implied volatility. Spot value: 2,372.81. Data: S&P500 options observed on 24/04/2017. Source Bloomberg.

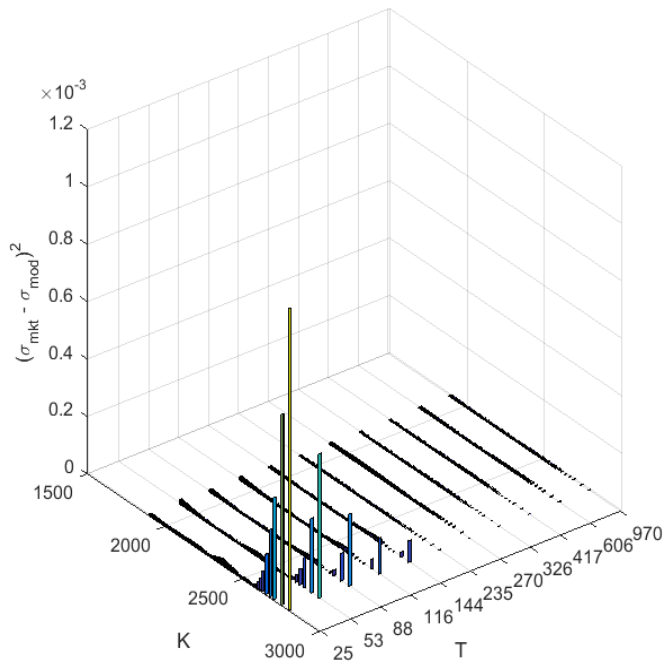


Figure C.4: 1SVFSE model calibration performance: 1-Day Calibration. Metrics: squared errors in volatility.  $\sigma_{mod}$ : model implied volatility.  $\sigma_{mkt}$ : market implied volatility. Spot value: 2,372.81. Data: S&P500 options observed on 24/04/2017. Source Bloomberg.

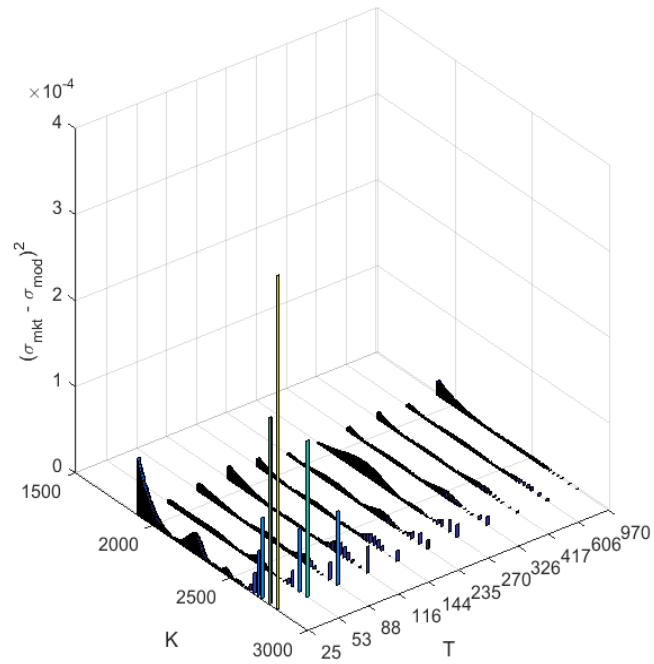


Figure C.5: 1SVFHO model calibration performance: 1-Day Calibration. Metrics: squared errors in volatility.  $\sigma_{mod}$ : model implied volatility.  $\sigma_{mkt}$ : market implied volatility. Spot value: 2,372.81. Data: S&P500 options observed on 24/04/2017. Source Bloomberg.

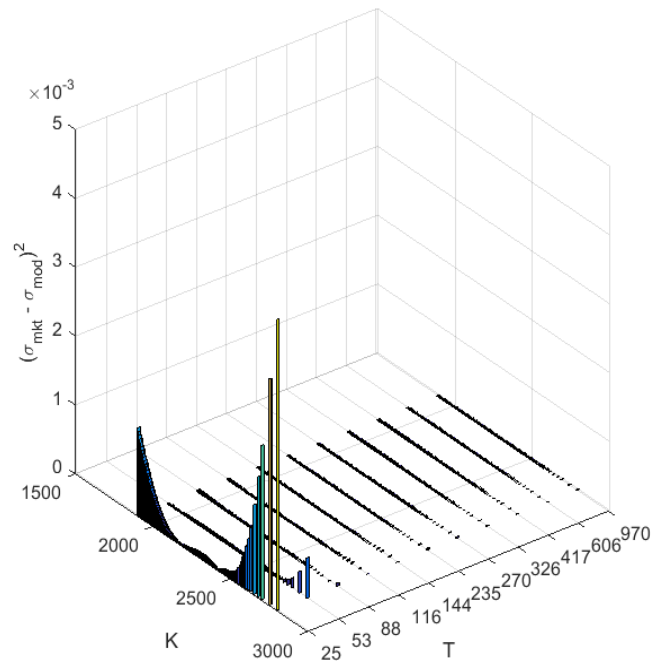


Figure C.6: Heston 2F model calibration performance: 1-Day Calibration. Metrics: squared errors in volatility.  $\sigma_{mod}$ : model implied volatility.  $\sigma_{mkt}$ : market implied volatility. Spot value: 2,372.81. Data: S&P500 options observed on 24/04/2017. Source Bloomberg.

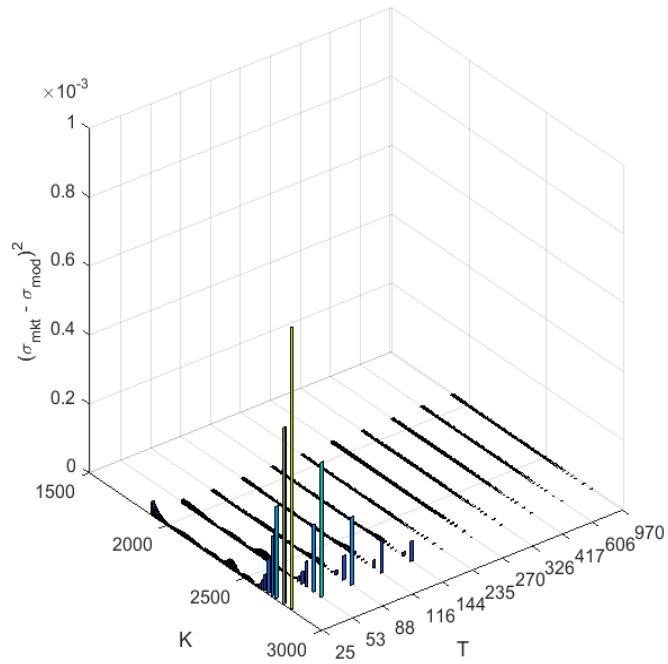


Figure C.7: 2SVFSE model calibration performance: 1-Day Calibration. Metrics: squared errors in volatility.  $\sigma_{mod}$ : model implied volatility.  $\sigma_{mkt}$ : market implied volatility. Spot value: 2,372.81. Data: S&P500 options observed on 24/04/2017. Source Bloomberg.

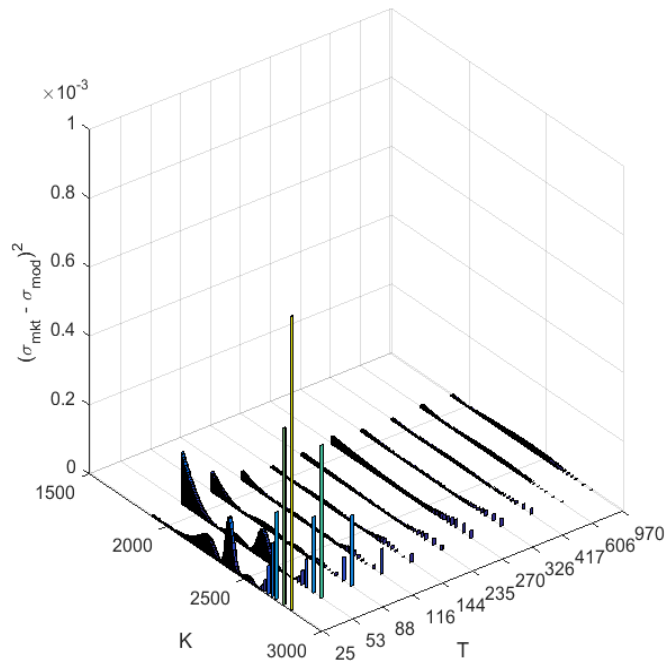


Figure C.8: 2SVFHOU model calibration performance: 1-Day Calibration. Metrics: squared errors in volatility.  $\sigma_{mod}$ : model implied volatility.  $\sigma_{mkt}$ : market implied volatility. Spot value: 2,372.81. Data: S&P500 options observed on 24/04/2017. Source Bloomberg.